The methyltransferases METTL7A and METTL7B confer resistance to thiol-based histone deacetylase inhibitors

Robert W. Robey[1,*], Christina M. Fitzsimmons[1,*], Wilfried M. Guiblet[1,8], William J.E. Frye[1], José M. González Dalmasy[1], Li Wang[2], Drake A. Russell[3], Lyn M. Huff[1], Andrew J. Perciaccante[1], Fatima Ali-Rahmani[1,9], Crystal C. Lipsey[1], Heidi M. Wade[1], Allison V. Mitchell[1], Siddhardha S. Maligireddy[1], David Terrero[4], Donna Butcher[5], Elijah F. Edmondson[5], Lisa M. Jenkins[1], Tatiana Nikitina[1], Victor B. Zhurkin[1], Amit K. Tiwari[4], Anthony D. Piscopio[6], Rheem A. Totah[3], Susan E. Bates[7], H. Efsun Arda[2], Michael M. Gottesman[1,#],Pedro J. Batista[1,#]

[1]Laboratory of Cell Biology, Center for Cancer Research, National Cancer Institute, National Institutes of Health, Bethesda, MD

[2]Laboratory of Receptor Biology and Gene Expression, Developmental Genomics Group, Center for Cancer Research, National Cancer Institute, National Institutes of Health, Bethesda, MD

[3]Department of Medicinal Chemistry, University of Washington, Seattle, WA

[4]Department of Pharmacology and Experimental Therapeutics, Department of Cancer Cell and Cancer Biology, University of Toledo, Toledo, OH

[5]Molecular Histopathology Laboratory, Frederick National Laboratory for Cancer Research, Frederick, MD, USA

[6]OnKure, Inc., Boulder CO

[7]Division of Hematology/Oncology, Department of Medicine, Columbia University Medical Center, New York, NY and Hematology/Oncology Research Department, James J. Peters Department of Veterans Affairs Medical Center, New York, NY

[8]Present address: Advanced Biomedical Computational Science, Frederick National Laboratory for Cancer Research, Frederick, MD

[9]Present Address: Roche Laboratories, Atlanta, GA

[#]To whom correspondence should be addressed

[*]These authors contributed equally to this work.

Classification(s): Biological Sciences; Pharmacology
Keywords: Drug resistance; HDAC; Methyltransferase

ABSTRACT

Histone deacetylase inhibitors (HDACis) are part of a growing class of epigenetic therapies used for the treatment of cancer. While elevated levels of the efflux pump P-gp are associated with *in vitro* resistance to romidepsin, this mechanism does not translate to the clinic. We developed a romidepsin-resistant cell line with a resistance mechanism independent of P-gp function that acts upstream of the deacetylation process. We found that expression of the methyltransferase METTL7A is necessary for resistance, and that expression of METTL7A in naïve cells can drive resistance to thiol-containing HDACis. We demonstrate that METTL7A can methylate romidesin *in vitro* and that the ability of METTL7A to drive resistance to thiol-containing HDACis can be blocked by the methyltransferase inhibitor DCMB. Our data supports a model whereby exposure of cells to romidepsin selects for upregulation of the methyltransferase METTL7A, which in turn modifies the zinc-binding thiol, inactivating the drug.

INTRODUCTION

Post-translational modification of histone tails via methylation, phosphorylation, or acetylation is an essential aspect of gene regulation in the cell [1]. Histone acetylation is controlled by the interplay between histone acetyltransferases (HATs) that catalyze the addition of acetyl groups to histones, and histone deacetylases (HDACs) that catalyze their removal. Increased histone acetylation leads to a more accessible chromatin configuration and increased gene transcription, while decreased histone acetylation is associated with transcriptional repression [2]. Alterations in the expression of HDAC proteins have been demonstrated in various cancers, potentially leading to altered transcriptional regulation of genes related to cell growth and differentiation [3]. Several HDAC inhibitors (HDACis) have been developed that can block histone deacetylation, thus resulting in increased histone acetylation via unrestrained HATs activity [4].

In clinical trials, HDACis have shown immense promise in the treatment of T-cell lymphoma. Two HDACis, vorinostat and romidepsin, have been approved as single agents by the United States Food and Drug Administration (FDA) for the treatment of cutaneous T-cell lymphoma [5-8]. Additionally, belinostat was approved as a single agent for the treatment of peripheral T-cell lymphoma [9] and tucidinostat (chidamide) has been approved in China as a single agent for the treatment of peripheral T-cell lymphoma [10]. Romidepsin is unique among the HDACis that have been approved for cancer treatment in that it is a bicyclic depsipeptide with an internal disulfide bond that must be reduced to form the activated molecule [11]. The reduced form of romidepsin

82 has two free sulfhydryl groups, one of which can coordinate with zinc in the active site of
83 HDACis, thus reversibly inhibiting the enzymes [11].
84
85 Despite dramatic responses to treatment in some T-cell lymphoma patients, romidepsin
86 can lose effectiveness after the initial response period. In addition, clinical trials with
87 solid tumors have been unsuccessful, suggesting intrinsic mechanisms of resistance.
88 Romidepsin was identified as a substrate of the ATP binding cassette transporter P-
89 glycoprotein (P-gp, encoded by the *ABCB1* gene) based on early studies with the NCI-
90 60 cell lines. Several groups have reported overexpression of P-gp in cell lines that are
91 selected for resistance to romidepsin [12-16]. However, in clinical samples, expression
92 levels of *ABCB1* did not predict response to romidepsin [17], prompting us to search for
93 non-P-gp mechanisms of resistance.
94
95 To generate a solid tumor model of romidepsin resistance, MCF-7 breast cancer cells
96 were selected with romidepsin and verapamil, an inhibitor of P-gp, to prevent the
97 emergence of P-gp as a resistance mechanism. While the resulting cell line, MCF-7
98 DpVp300, was selectively resistant to romidepsin, it did not overexpress P-gp. As such,
99 resistance of DpVp300 cells to romidepsin is not driven by P-gp. We performed Assay
100 for Transposase-Accessible Chromatin sequencing (ATAC-seq) and RNA-sequencing
101 (RNA-seq) on MCF-7 and MCF-7 DpVp300 cells to identify possible mechanisms of
102 resistance. One of the genes that was most upregulated in MCF-7 DpVp300 cells
103 compared to MCF-7 cells was *METTL7A*, a putative methyltransferase. This gene was
104 also found to be upregulated in HuT78 DpVp50 and HuT78 DpP75 cells, two

105 romidepsin-resistant T-cell lymphoma cell lines we had generated previously [18]. Here,
106 we demonstrate that METTL7A overexpression can confer resistance not only to
107 romidepsin, but to other HDACis that have a thiol as the zinc-binding moiety.
108 Expression of the close homolog METTL7B can also confer resistance to HDACis
109 bearing a thiol group, albeit with less efficiency. Overexpression of these
110 methyltransferases represents a previously unknown mechanism of resistance to thiol-
111 based HDACis and a potential target to improve HDACi-based therapies.
112

113 **RESULTS**

114 *MCF-7 DpVp300 cells are selectively resistant to romidepsin*

115 The MCF-7 DpVp300 cell line was generated via prolonged selection of MCF-7 cells
116 with romidepsin in the presence of the P-gp inhibitor verapamil to prevent any selection
117 benefit from P-gp overexpression. To determine which drugs the MCF-7 DpVp300 cells
118 are sensitive or resistant to (the cross-resistance profile), cytotoxicity assays were
119 performed with several chemotherapeutic agents, including HDACis. Interestingly, the
120 DpVp300 cell line was much more resistant to romidepsin (Fig. 1A, on average 218-fold
121 more resistant) and much less resistant to other HDACis, such as belinostat (8-fold),
122 panobinostat (2.5-fold), and vorinostat (5-fold). Additionally, the MCF-7 DpVp300 line
123 was not cross resistant to other chemotherapeutic agents such as 5-FU, methotrexate,
124 teniposide, or topotecan, exhibiting no more than 3-fold more resistance to those
125 compounds than MCF-7 cells (Supplemental Table S1).
126

127 As HDACi treatment results in increased levels of acetylated histones and p21
128 transcription [19] , we examined the effect of HDACis on global histone acetylation and
129 p21 levels. MCF-7 and MCF-7 DpVp300 cells were treated with romidepsin, belinostat,
130 panobinostat, or vorinostat for 24 h after which protein was extracted and subjected to
131 analysis by immunoblot. MCF-7 cells treated with any of the HDACis displayed
132 increased levels of acetylated histone H3 and p21 compared to untreated cells (Fig.
133 1B). In contrast, MCF-7 DpVp300 cells treated with romidepsin did not exhibit the
134 increased levels of acetylated histone H3 or p21 that were found with MCF-7 cells;
135 however, treatment with the other HDACis resulted in higher levels of acetylated histone
136 H3, which suggested a resistance mechanism that is specific to romidepsin and acts
137 upstream of the deacetylation process.
138
139 Treatment of cancer cell lines with HDACis is known to cause cell cycle perturbations,
140 with some cell lines demonstrating a G_1/G_0 arrest and others a G_2/M arrest, depending
141 upon which checkpoints were most intact [20-22]. Cell cycle analysis was performed on
142 MCF-7 and DpVp300 cells treated with belinostat, romidepsin, panobinostat, or
143 vorinostat for 24h as outlined above. In the MCF-7 cells treated with the HDACis, a
144 decrease of cells in the G_1/G_0 phase and an increase in cells in the G_2/M phase was
145 observed (Supplemental Fig. S1A). While a similar pattern was observed in MCF-7
146 DpVp300 cells when treated with belinostat, panobinostat or vorinostat, no such
147 changes were observed with romidepsin treatment. When data from three independent
148 experiments were compiled (Fig. 1C), we observed a significant decrease in the
149 percentage of cells in the G_1/G_0 and S phases of the cell cycle and an increase of cells

150 in the G_2/M phase in MCF-7 cells treated with any of the HDACis. Similar changes were
151 observed when DpVp300 cells were treated with belinostat, panobinostat or vorinostat;
152 however, romidepsin treatment did not produce significant changes (Fig. 1C).
153
154 To examine the effects of higher doses of romidepsin, we treated MCF-7 and DpVp300
155 cells with increasing concentrations of romidepsin for 24 h and examined levels of
156 histone acetylation and p21 by immunoblot. We observed that MCF-7 cells displayed
157 increased levels of histone H3 acetylation when treated with as little as 1 ng/ml
158 romidepsin (Fig. 1D). In contrast, increased histone acetylation was not observed until
159 MCF-7 DpVp300 cells were treated with at least 100 ng/ml romidepsin. Based on these
160 results, we concluded the resistance mechanism present in MCF-7 DpVp300 cells
161 protected the cells from romidepsin levels at least 100 times higher than MCF-7 cells –
162 consistent with the earlier observation in cytotoxicity assays that MCF-7 DpVp300 cells
163 are at least 200-fold resistant to romidepsin (Fig. 1A).
164
165 *P-gp is not responsible for romidepsin resistance in MCF-7 DpVp300 cells*
166 We and others have demonstrated that selection with romidepsin as a single agent
167 leads to overexpression of P-gp as a resistance mechanism [13, 15, 16, 23]. The MCF-
168 7 DpVp300 line was generated to identify alternative mechanisms of resistance,
169 blocking P-gp activity with verapamil to prevent its emergence as a resistance
170 mechanism. To confirm that P-gp does not play a role in romidepsin resistance in the
171 DpVp300 cell line, surface expression of P-gp was measured by flow cytometry using
172 the UIC2 antibody. P-gp was readily detected in the *ABCB1*-transfected MDR-19 cell

173 line, as shown by the difference in fluorescence between the isotype control peak (solid
174 line) and UIC-2 peak (dashed line) (Supplemental Fig. S1B). However, P-gp was largely
175 undetected in the empty vector transfected line, as shown by the overlapping isotype
176 control (solid line) and UIC-2 peak (dashed line). We did not detect P-gp expression in
177 either the MCF-7 cells or in MCF-7 DpVp300 cells, as shown by the overlapping isotype
178 control (solid line) and UIC-2 (dashed line) peaks. Cross-resistance to romidepsin in the
179 MDR-19 line compared to empty vector transfected cells leads to approximately the
180 same degree of resistance as that observed between DpVp300 cells and MCF-7 cells
181 (Supplemental Fig. S1C). Thus, we concluded the mechanism of resistance at work in
182 the MCF-7 DpVp300 cells is P-gp-independent.
183
184 *MCF-7 DpVp300 cells have significant changes in gene expression*
185 Both MCF-7 DpVp300 and HuT78 DpVp50 cells, which we previously generated [18],
186 have acquired mechanisms of resistance to romidepsin that do not involve P-gp/ABCB1
187 function. To determine which molecular pathways might be involved in the resistance
188 mechanism we assessed changes in gene expression between the sensitive and the
189 drug-resistant cells.
190 We observed significant changes in steady-state mRNA levels between the sensitive
191 and DpVp cell lines (Fig. 2A) for both MCF-7 and Hut78. Approximately 500 genes were
192 upregulated, and 180 genes were downregulated ($|l2fc| > 1.0$ and $padj < 0.05$) in both
193 HuT78 and MCF-7 DpVp cells. The majority of GO-terms enriched for up- or down-
194 regulated genes were distinct between the two cell lines and offered no indication of
195 underlying genes or molecular pathways that could drive resistance to romidepsin

196 (Supplemental Fig. S2A). As expected, we observed little change in the expression level
197 of *ABCB1* mRNA. We focused our analysis on the genes most up-regulated in both the
198 MCF-7 and HutT78 cells. We identified 5 genes that are highly up-regulated in both
199 DpVp variants (log2 fold change >= 5.0 and padj < 1e-300) (Fig. 2B). These genes
200 include *PEG10*, *PRAME*, *SEMA3A*, *SGCE*, and *METTL7A*. We decided to focus on
201 METTL7A, a putative methyltransferase that has not been extensively studied but has
202 been linked to lipid droplet formation in cells [24]. METTL7B, a paralog of METTL7A, is
203 an alkyl-thiol methyltransferase that is capable of methylating thiol groups of various
204 compounds such as captopril, hydrogen sulfide, and dithiothreitol [25]. As the active
205 form of romidepsin contains a thiol as the zinc binding group, and methylation of the
206 thiol group would prevent coordination of the molecule with zinc in the HDAC binding
207 pocket, we hypothesized that METTL7A might be able to inactivate romidepsin or other
208 HDACis with a thiol as the zinc-binding group. Immunoblot analysis confirmed high
209 levels of METTL7A protein not only in MCF-7 DpVp300 and HUT78 DpVp50 cells but
210 also in another resistant cell line, HuT78 DpP75 [18] (Fig. 2C). Taken together, these
211 results indicate that METTL7A is upregulated in both MCF-7 DpVp300 and HuT78
212 DpVp50 and may play a role in romidepsin resistance.
213
214 *METTL7A is upregulated at the transcriptional level*
215 Several mechanisms could drive upregulation of METTL7A in DpVp cells. To determine
216 if expression of METTL7A is regulated at the level of transcription, we compared
217 chromatin accessibility in the parent and the DpVp lines for MCF-7 and HuT78. A total
218 of 19,937 differentially open regions (DORs) (padj < 0.05) in the MCF-7 cells and

219 34,737 DORs in the HuT78 cells were identified (Fig. 2D). Consistent with our
220 observation that there is little overlap between up- and down-regulated genes at the
221 mRNA level, we also observe little overlap between MCF-7 and HuT78 DpVp DORs,
222 with only 737 DORs common to both DpVp cell lines (Fig. 2E). *De novo* motif discovery
223 of transcriptional binding sites at DORs shows little overlap between the two cell lines,
224 (Supplemental Fig. S2B), suggesting different transcriptional networks are active in the
225 two DpVp cell lines. As expected, genes associated with highly accessible DORs tend
226 to be upregulated in the DpVp cells (Fig. 2F). Finally, upregulation of METTL7A is
227 associated with open DORs at the genomic locus (Figure 2G) and an increase in
228 density of subnucleosomal DNA fragments (Supplemental Fig 2C). The mRNA coding
229 for METTL7A has been shown to undergo extensive editing at the 3' end, and protein
230 expression has been shown to be suppressed by adenosine deaminase acting on RNA
231 (ADAR1/2) and miR-27a [32]. We observe extensive editing of the 3'-UTR of METTL7A
232 in both of our resistance models (Supplemental Fig. S2D), suggesting that post-
233 transcriptional regulation might also play a role in the upregulation of METTL7A.
234
235 *MCF-7 DpVp300 cells are resistant to other thiol-based HDACIs*
236 Since METTL7B has been shown to be an alkyl-thiol methyltransferase, we
237 hypothesized that if METTL7A is the driver of romidepsin resistance, the MCF-7
238 DpVp300 might be resistant to other HDACis with a thiol group. We performed
239 cytotoxicity assays on MCF-7 and MCF-7 DpVp300 cells with largazole, a natural-
240 product HDACi [26]; OKI-005, an HDACi based on the structure of largazole and
241 currently in clinical trials [27]; KD5170, a class I and II HDACi [28]; and NCH-51, an

242 HDACi based on the structure of vorinostat [29]. All of these small molecules are
243 thioester prodrugs that hydrolyze to yield a thiol as the zinc binding group. We found
244 that the DpVp300 cells were resistant to all the thiol-based HDACis tested (Fig. 3A and
245 Supplementary Table S2).
246 Immunoblot analysis of histone acetylation and p21 expression showed that while
247 acetylated histone H3 and p21 expression increased when MCF-7 cells were treated
248 with any of the above thiol-based HDACis, no increase in expression of these proteins
249 was observed in DpVp300 cells treated with any of the HDACis (Fig. 3B). This suggests
250 that MCF-7 DpVp300 cells were selectively resistant to the effects of thiol-based
251 HDACis. Further, these results support the hypothesis that METTL7A methylates and
252 inactivates thiol-based HDACis, driving resistance to treatment.
253
254 *Knockout of METTL7A in MCF-7 DpVp300 cells restores sensitivity to thiol-based*
255 *HDACIs*
256 To investigate whether METTL7A was responsible for the observed resistance to
257 romidepsin and other HDACis with an active thiol group, we performed CRISPR-Cas9-
258 mediated knockout of *METTL7A*. We generated two clones that were completely
259 negative for METTL7A expression, 7A KO B1 and 7A KO B3, as well as one clone that
260 had reduced expression but not total loss of METTL7 protein, 7A KO B4 (Fig. 4A).
261 When the clones were treated with romidepsin for 24 h, the ability of romidepsin to
262 induce histone H3 acetylation and p21 was restored in the complete knockouts while
263 little effect was observed in the clone with partial knockdown (Fig. 4A). In cytotoxicity
264 assays, sensitivity to all thiol-based HDACis was restored nearly to the level of parent

265 MCF-7 cells in the knockout clones, while resistance to the HDACis was only slightly
266 decreased in the partial knockdown clone (Fig. 4B). Sensitivity to vorinostat, which does
267 not contain a thiol group, was unchanged (Supplemental Table S3).
268 MCF-7, MCF-7 DpVp300 and 7A KO B1 cells were subsequently treated with
269 romidepsin, KD-5170, largazole, NCH-51, or OKI-005 for 24 h, after which the effects on
270 histone acetylation and p21 expression were examined by immunoblot (Fig. 4C). While
271 MCF-7 cells displayed increases in histone acetylation and p21 after treatment with any
272 of the HDACis, no increases were observed in MCF-7 DpVp300 cells, and knockout of
273 METTL7A restored the ability of the thiol-based HDACis to induce histone acetylation
274 and p21.
275
276 In addition, we performed cell cycle analysis on MCF-7, MCF-7 DpVp300 cells and the
277 3 knockout clones (Fig. 4D and Supplemental Fig. S3). Cells were treated at the
278 concentrations used above for the immunoblot for 24 hrs. We observed that MCF-7
279 cells had fewer cells in the G_1/G_0 and S phases of the cell cycle and an increased
280 number of cells in G_2/M phase after treatment with any of the compounds (Fig. 4D).
281 Changes in the cell cycle were not observed in DpVp300 cells treated with any of the
282 drugs except in the case of NCH-51. In agreement with the cytotoxicity data, we
283 observed significant cell cycle perturbations after treatment with the thiol-based HDACis
284 in both METTL7A knockout clones. These effects were comparable to what we
285 observed with MCF-7 cells. In the partial knockout clone, we noted some significant cell-
286 cycle changes; however, these changes were less pronounced compared to MCF-7
287 cells, suggesting that even a low level of METTL7 expression is still protective to the

288 cells. These results all pointed to METTL7A as a mediator of resistance to HDACis with
289 a thiol as the zinc-binding moiety.
290
291 *Overexpression of METTL7A or METTL7B confers resistance to thiol-based HDACis*
292 To further test the ability of METTL7A to confer resistance to thiol-containing HDACis,
293 we transfected HEK-293 cells, which are sensitive to HDACis, with *METTL7A* and the
294 close paralog *METTL7B*. We selected two clones of each with comparable protein
295 levels of METTL7A or METTL7B (Fig. 5A) and performed three-day cytotoxicity assays
296 with largazole, OKI-005, romidepsin, NCH-51 or KD5170 along with two non-thiol HDAC
297 inhibitors, vorinostat and mocetinostat. METTL7A overexpression conferred resistance
298 to all thiol-based HDACis tested (Fig. 5B and Supplemental Table S4) compared to
299 empty vector transfected cells (Vector). METTL7B overexpression conferred low-level
300 resistance to romidepsin and it also appeared to be less effective than METTL7A for
301 largazole and KD5170 (Fig. 5B).
302
303 We next treated HEK-293 cells transfected with empty vector (Vector) or one of the
304 METTL7A (7A 1-2) and METTL7B (7B 2-2) clones with romidepsin, KD-5170, largazole,
305 NCH-51, or OKI-005 for 24 h and examined changes in histone acetylation and p21
306 expression. In agreement with cytotoxicity assays, cells expressing METTL7B were not
307 resistant to the effects of romidepsin and displayed increased levels of acetylated
308 histone H3 and p21, while cells expressing METTL7A were resistant to the effects of all
309 the thiol-based HDACis (Fig. 5C).
310

311 Cell cycle analysis was also performed on the transfected cells after treatment with
312 romidepsin, KD-5170, largazole, NCH-51, or OKI-005 for 24 h. As was observed with
313 MCF-7 cells, all thiol-based HDACs induced cell cycle changes in empty-vector
314 transfected cells, causing a decrease in the number of cells in the G_1/G_0 and S phases
315 and an increase in the number of cells in the G_2/M phase (Supplemental Fig. S4). In
316 contrast, no significant cell cycle changes were observed in cells transfected to express
317 METTL7A. In the METTL7B clones, while no significant cell cycle changes were
318 observed with a majority of the thiol-based HDACs, we did note significant cell cycle
319 perturbations in cells treated with romidepsin and KD-5170 (Fig. 5D).
320
321 *Evidence of methylated romidepsin in culture media*
322 If METTL7A can methylate romidepsin, we rationalized that we should observe
323 methylated romidepsin in the culture medium of MCF-7 DpVp300 cells incubated with
324 the drug. Using liquid-chromatography coupled to tandem-mass spectrometry (LC-
325 MS/MS) we observed high levels of dimethylated romidepsin in the media of MCF-7
326 DpVp300 cells (Fig. 6A), whereas much lower levels were observed in the media of
327 MCF-7 cells and the two METTL7A knockout clones, supporting the hypothesis that
328 METTL7A can methylate and inactivate romidepsin.
329
330 The ability of METTLA and METTL7B to methylate romidepsin was also examined in a
331 cell-free system. Recombinant METTL7A and METTL7B were incubated with reduced
332 romidepsin for 2 hours and mass spectrometry performed to quantify any
333 monomethylate reduced romidepsin. Both METTL7A and METTL7B were found to

334 methylate reduced romidepsin (Fig. 6B). In contrast, no methylated product, or trace
335 amounts was noted when the reactions were performed in the absence of the methyl
336 donor S-adenosyl-L-methionine (SAM), or when the enzyme was pre-treated with
337 boiling. Together, these results confirm the methyltransferase activity of these enzymes
338 using romidepsin as a substrate.
339
340 The phenylethanolamine-N-methyltransferase inhibitor 2,3-Dichloro-α-
341 methylbenzylamine hydrochloride (DCMB) was recently reported to selectively inhibit
342 the methyltransferase activity of METTL7A but not METTL7B [30]. We therefore
343 conducted cytotoxicity assays in cells over expressing METTL7A or METTL7B
344 combining DCMB and NCH-51, since NCH-51 was found to be a substrate of both
345 METTL7A and METTL7B. Using a non-toxic concentration of DCMB we found that
346 DCMB completely reversed resistance to NCH-51 mediated by METTL7A but not
347 METTL7B. Inhibitors of other methyltransferases could also be potential inhibitors of
348 METTL7A and METTL7B and may reverse resistance to thiol-based HDACis.
349
350 *Tissue expression of METTL7A and METTL7B*
351 While our work with resistant cells implicates METTL7A in resistance to HDACis, its
352 physiological role in development and homeostasis remains to be determined. To
353 understand the localization of METTL7A and METTL7B within tissues, we performed
354 immunohistochemistry on normal tissue microarrays. Both METTL7A and METTL7B
355 were found to be highly expressed in hepatocytes (Fig 7A and 7B, respectively) and
356 distinct segments of the nephron (Fig. 7C and 7D), while METTL7B was found in the

357 intestinal enterocytes (Fig. 7E and 7F) and METTL7A was found in breast epithelium
358 (Fig. 7G and 7H). METLL7A is also highly expressed in glial cells, certain nephron
359 segments, and Leydig cells of the testes, while METTL7B is highly expressed in
360 enterocytes, neurons, and certain nephron segments. Modest expression of both
361 METTL7A and METTL7B is also found in cardiomyocytes, gastric mucosa, and
362 subcutaneous adipocytes (Sup. Table 5). The localization pattern of METTL7A and
363 METTL7B is consistent with a role in detoxification, which might have treatment
364 implications for drugs in this class.
365

366 **DISCUSSION**

367 Precise control of gene expression through acetylation and deacetylation of lysine
368 residues within the tails of histones is important for timely expression of genes, and this
369 epigenetic regulation is frequently dysregulated in cancers (reviewed in [31]). HDACis
370 are a novel class of chemotherapeutic drugs that modulate the acetylation levels of
371 histones by coordinating with Zn^{2+} in the catalytic pocket of HDACs, thus inhibiting
372 enzyme activity. Reduced HDAC activity results in hyperacetylation of substrates and
373 induces downstream cell cycle arrest or apoptosis. Vorinostat and romidepsin were the
374 first FDA-approved HDACis for the treatment of T-cell lymphomas [5-7, 32]. Despite
375 dramatic responses in some patients, romidepsin is not always effective and resistance
376 can develop after responses. Furthermore, the activity of HDACis in solid tumors has
377 been limited, suggesting intrinsic mechanisms of resistance. While elevated levels of
378 the efflux pump P-gp are associated with *in vitro* resistance to romidepsin, this
379 mechanism does not translate to the clinic [17]. Thus, we set out to identify mechanisms

380 of resistance to HDACis. Here, we identify overexpression of the putative
381 methyltransferases METTL7A and METTL7B as a mechanism of drug resistance to
382 thiol-based HDACis (Fig. 7I).
383
384 In this study, we identified overexpression of METTL7A as a mechanism of romidepsin
385 resistance in two different cell models. In both models, we uncovered a mechanism of
386 resistance that is independent of P-gp function and acts upstream of the deacetylation
387 process. Expression of the methyltransferase METTL7A is necessary for resistance,
388 and expression of METTL7A in naïve cells can drive resistance to thiol-containing
389 HDACis. METTL7A-dependent resistance to romidepsin correlated with the presence of
390 methylated drug in cell media, and the ability of METTL7A to drive resistance to thiol-
391 containing HDACis can be blocked by the methyltransferase inhibitor DCMB. Finally,
392 METTL7A can methylate romidesin *in vitro*. Our data supports the model whereby
393 exposure of cells to romidepsin selects for upregulation of the methyltransferase
394 METTL7A. Once expressed, METTL7A methylates the zinc-coordinating thiol to
395 prevents the drug from inhibiting HDAC, rendering the cells resistant to this class of
396 therapeutic agents. We have noted that the cells selected for high levels of resistance to
397 romidepsin are also resistant, albeit to a lesser extent, to other HDACis that do not
398 contain thiol groups. This suggests that one or more factors in the resistant cells
399 promote more general resistance to HDACis. Whether these are mediated by some of
400 the other molecular changes we have observed in these cells remains to be determined.
401

402 Several mechanisms might be involved in METTL7A upregulation. As previously
403 described [33], we observe extensive editing of the 3′-UTR of METTL7A in both of our
404 resistance models (Supplemental Fig. S2D), suggesting that post-transcriptional
405 regulation may play a role in the up-regulation of METTL7A. We also observe changes
406 in chromatin accessibility at the METTL7A locus that support up-regulation of METTL7A
407 at the transcriptional level. The upregulation in METTL7A transcription in the DpVp
408 cells could be driven by changes in transcriptional networks, changes in DNA
409 methylation at CpG sites in the METTL7A gene body, or both. In thyroid cancer,
410 expression of METTL7A has been shown to be regulated by methylation of a CpG
411 island at exon 2 of *METTL7A* [34]. Since HDACis have been shown to affect DNA
412 methylation [35-37], one hypothesis is that exposure to HDACis results in a reduction of
413 DNA methylation at the METTL7A locus that allows for the expression of the METTL7A
414 mRNA.
415 Few studies have linked expression of METTL7A or METTL7B to drug resistance. Jun
416 and colleagues identified METTL7A as a mechanism of resistance in methotrexate
417 resistant choriocarcinoma cells [38]. However, when we performed cytotoxicity assays
418 with methotrexate on MCF-7 and DpVp300 cells, we did not find increased resistance in
419 the DpVp300 line. Additionally, we note that methotrexate does not contain thiol groups.
420 Thus, other potential factors besides METTL7A may be involved in methotrexate
421 resistance. A role for METTL7B in resistance to tyrosine kinase inhibitors has been
422 suggested by Song and colleagues who noted increased expression of METTL7B in
423 lung adenocarcinoma cell lines that were resistant to the tyrosine kinase inhibitors
424 (TKIs) gefitinib or osimertinib [39]. In their report, METTL7B was not found to directly

425 interact with the TKIs, rather METTL7B overexpression was associated with increased
426 antioxidant capacity and reactive oxygen species (ROS) scavenging [39].
427
428 While two previous studies suggested METTL7A methylates RNA [40] and DNA [41],
429 our studies, in line with the work of Totah and colleagues on both METTL7A [30] and
430 the close paralog METTL7B [25], suggest that METTL7A directly methylates thiol
431 groups on small molecules in the cell.
432
433 While we observed that both METTL7A and METTL7B were able to methylate
434 romidepsin in a cell-free system, experiments with our cell line models suggests that the
435 two paralogs have different roles in drug resistance, with METTL7A being the relevant
436 driver of resistance to romidepsin. Several reasons can explain this discrepancy and
437 warrant further investigation. Differences in reaction site preferences, post-translational
438 modifications, binding partners, or sub-cellular localization between the two enzymes
439 could results in differences in activity toward romidepsin.
440
441 While our work reveals a role for METTL7A and METTL7B in drug resistance, the
442 function of these methyltransferases during development and a physiological role for
443 them remains to be elucidated. One of the murine homologs of METTL7A, Mettl7a1, is
444 transiently and significantly upregulated during reprogramming of mouse embryonic
445 fibroblasts (MEFs) to induce endoderm progenitors [42]. Addition of Mettl7a1 to the
446 reprogramming cocktail enhanced conversion of MEFs into induced endoderm
447 progenitors by promoting reprogramming efficiency. METTL7A also plays a role in

448 osteogenic differentiation by mediating the effects of glucose on cell survival and
449 osteogenic induction [41]. Lastly, a role in hydrogen sulfide homeostasis has also been
450 proposed for both METTL7A and METTL7B [25, 30]. Both paralogs are expressed in
451 the stomach, kidney, and liver which may suggest a detoxifying role for these proteins
452 under normal physiological conditions.
453
454 The data presented here show that METTL7A has the ability to inactivate thiol-
455 containing HDAC inhibitors before they reach their targets. It is possible that this
456 mechanism of resistance, despite the potential to reduce effective drug concentrations
457 in cancer cells, reduces the systemic effects of the drugs given to patients. The key
458 challenge in oncopharmacology is that we do not always know if a drug reached its
459 target. How much the presence of METTL7A is responsible for the inability to translate
460 the unique activity seen in T-cell lymphomas to solid tumors remains to be investigated
461 ([43-46]). We can further hypothesize a role in the emergence of resistance in T-cell
462 lymphomas, and this remains to be investigated as well. Together, these findings are a
463 reminder of just how much remains to be learned and solved regarding how cancers
464 become resistant to treatment.
465

466 **ACKNOWLEDGEMENTS**

467 We thank members of the Batista, Gottesman and Arda Labs for discussion and critical
468 reading of the manuscript. The authors thank the Center for Cancer Research (CCR)
469 Genomics Core in Bethesda, Maryland, as well as the CCR Sequencing Facility in
470 Frederick, Maryland, for help with high-throughput sequencing. This work utilized the
471 computational resources of the NIH HPC Biowulf cluster (http://hpc.nih.gov). We
472 appreciate the editorial assistance of George Leiman. The views expressed in this
473 article are those of authors and may not reflect the official policy or position of the
474 National Institute of Health, Department of the Army, Department of Defense. Mention
475 of trade names, commercial products, or organizations imply endorsement by the U.S.
476 Government. Supported by the Intramural Research Program at the National Cancer
477 Institute (NCI) of the National Institutes of Health. A.K.T. is supported by Department of
478 Defense – BCRP Level 2 award (1W81XWH-21-1-0053). C.M.F. is partially supported
479 by a Postdoctoral Fellowship from the American Cancer Society (PF-19-157-01-RMC).
480 Authors' Discosures: Anthony D. Piscopio is CEO and president of OnKure, Inc

481

482 **HIGH-THROUGHPUT SEQUENCING DATA AND CODE AVAILABILITY**

483 RNA-seq and ATAC-seq data were deposited in the Gene Expression Omnibus
484 database GSE217130. Code and scripts used to generate data and plots are available
485 at https://github.com/BatistaLab/METTL7A

486

487 **MATERIALS AND METHODS**

488 *Chemicals*

489 Methotrexate, 5-fluoruracil, teniposide, apicidin, trichostatin a, and topotecan were
490 obtained from Sigma Aldrich (St. Louis, MO). Romidepsin was obtained from Selleck
491 Chem (Houston, TX). Belinostat, mocetinostat, and panobinostat were purchased from
492 ChemieTek (Indiannapolis, IN). Dacinostat, resminostat, pracinostat, chidamide,
493 vorinostat, entinostat, NCH-51, and KD 5170 were obtained from Cayman Chemical
494 (Ann Arbor, MI). Rocilinostat was purchased from ApexBio Technology (Houston, TX).
495 PCI-34051 was from Tocris (Minneapolis, MN). Largazole and OKI-005 were
496 synthesized in-house by OnKure.
497
498 *Cells*
499 MCF-7 breast cancer cells were selected in increasing concentrations of romidepsin to
500 generate the MCF-7 DpVp300 cell line that is maintained in 300 ng/ml romidepsin with 5
501 µg/ml verapamil. The HUT78 cell line was purchased from ATCC (Manassas, VA) and
502 the romidepsin-resistant HUT78 DpVp50 and DpP75 cell lines have been previously
503 described [18]. All cells were cultured in RPMI-1640 supplemented with 10% FCS and
504 Pen/Strep. HEK293 cells were also from ATCC and were maintained in Eagle's
505 minimum essential medium with 10% FCS and Pen/Strep. HEK293 cells were
506 transfected with empty pcDNA3.1 vector, or vector containing full-length *METTL7A* or
507 *METTL7B* with a C-terminus FLAG tag (all vectors from Genscript, Piscataway, NJ)
508 using Lipofectamine 2000 (Thermo Fisher Scientific, Waltham, MA) according to the
509 manufacturer's instructions. Clones were selected and were maintained in 1 mg/mL
510 G418. CRISPR-mediated knockout of METTL7A from MCF-7 DpVp300 cells was
511 achieved by co-transfecting knockout and homology directed repair vectors for

512 METTL7A (obtained from Santa Cruz Biotechnology, Dallas, TX) using Lipofectamine
513 2000 and subsequent selection with puromycin (3 µg/ml). Clones were then isolated
514 and characterized for loss of METTL7A protein via immunoblot.
515
516 *Cytotoxicity assays*
517 Cells were plated at a density of 5000 cells/well in opaque, white 96-well plates and
518 allowed to attach overnight. The next day drugs were added, and plates were incubated
519 for 3 days after which CellTiterGlo (Promega, Madison, WI) was added according to the
520 manufacturer's instructions. Plates were read on a Tecan Infinite M200 Pro (Tecan
521 Systems, Inc., San José, CA).
522
523 *Immunoblot analysis*
524 Whole cell lysates were obtained by harvesting cells in RIPA buffer and sonicating
525 samples in an inverted cup horn sonicator for 3 bursts of 30 sec, after which the
526 samples were centrifuged at 10000 RPM for 10 min and soluble proteins were removed.
527 When examining histone acetylation, RIPA buffer additionally contained 500 nM
528 trichostatin A to inhibit histone deacetylases after lysing cells. Protein lysates (approx.
529 15-20 µg) were separated by PAGE and transferred to nitrocellulose membranes that
530 were subsequently probed with antibodies against total histone H3 (cat# 05-499,
531 Millipore-Sigma, Burlington, MA), pan-Acetyl histone H3 (cat# 06-599, Millipore-Sigma),
532 METTL7A, METTL7B, beta-actin, (generated in mouse cat# 3700, or rabbit cat# 4970,
533 Cell Signaling Technology, Danvers, MA) and p21 (cat# 2946, Cell Signaling). Anti-
534 FLAG antibody (cat# F1804-200UG) was from also from Millipore-Sigma.

535

536 *Flow cytometry*

537 To determine surface expression of P-glycoprotein, trypsinized cells were incubated
538 with phycoerythrin-labeled UIC2 antibody or phycoerythrin-labeled isotype control IgG2a
539 kappa (both from ThermoFisher, Grand Island, NY) for 20 min at room temperature in
540 2% bovine serum albumin/PBS. Cell fluorescence was measured with a FACSCanto
541 flow cytometer (BD Biosciences, San José, CA) and data analysis was performed using
542 FloJo v10.4.2 (FlowJo LLC, Ashland OR). At least 10,000 events were collected per
543 sample. For cell cycle analysis, cells were plated and allowed to attach overnight before
544 being treated with HDACIs for 24 h. Cells were then harvested by trypsinization,
545 centrifuged, and the supernatant removed. Cell pellets were resuspended in equal
546 volumes of staining solution (0.05 mg/ml propidium iodide and 0.1% Triton X) and
547 RNAse A solution (200 U/mL RNAse A in deionized water). Cells were stained for 20
548 min and were subsequently read on a FACSCanto Flow Cytometer with at least 10,000
549 events collected per sample. The percentage of cells in each phase of the cell cycle
550 was determined by Modfit LT for Mac version 5.0 (Verity Software House, Topsham,
551 ME). Statistically significant changes in the percent of cells in each phase of the cell
552 cycle was determined by a one-way ANOVA test with a correction for multiple
553 comparisons.

554

555 *RNA sequencing analysis*

556 RNA was extracted from the MCF-7, MCF-7 DpVp300, HuT78, HuT78 DpVp50 and
557 HuT78 DpP50 cell lines using the RNeasy kit from Qiagen (Germantown, MD). RNA

558 sample integrity and quantity for three biological replicates were assessed by the Center
559 for Cancer Research Genomics Core using RNA ScreenTape Analysis (Agilent). All
560 RNA samples had RNA Integrity Numbers of (> 8.0). RNA libraries were generated
561 using a TruSeq Stranded mRNA library prep kit (Illumnia) and paired-end RNA
562 sequencing (2 x 75) was performed by the CCR Sequencing Facility and Genomics
563 Technology Core on a NextSeq 500 Sequencing System. Read quality analysis was
564 performed using FASTQC. Reads of the samples were trimmed for adapters and low-
565 quality bases using Cutadapt (version 2.3) before alignment with the hg38 reference
566 genome using Spliced Transcripts Alignment to a Reference (version 2.7.0f). The
567 number of reads mapping to each transcript was determined with HTseq-count (version
568 0.9.1). Differential expression was determined using DESeq2 (version 1.26.0) within the
569 R Studio (version 3.6.3).
570
571 *Omni-ATAC-seq assay*
572 Library Generation
573 Approximately 20,000 cells per sample were used for omni ATAC-seq assay following
574 the protocol described in Corces et al. [47] with minor modifications. For each cell line,
575 two biological replicates were included for control and resistant lines, respectively. To
576 isolate the nuclei, cells were resuspended in cold ATAC-Resuspension Buffer (RSB)
577 containing 0.1% NP40, 0.1% Tween-20, and 0.01% Digitonin, and incubated on ice for
578 3 minutes. The lysis was washed out by addition of 1 mL of RSB containing 0.1%
579 Tween-20 and mixed by inverting tubes. The nuclei were then pelleted at 500RCF for
580 10 minutes at 4C. For transposition, each nuclei pellet was resuspended in 50 µL of

581 transposition mix (25 µl 2x TD buffer, 2.5 µl transposase (100 nM final), 16.5 µl PBS,
582 0.5 µl 1% digitonin, 0.5 µl 10% Tween-20, 5 µl H_2O) and incubated at 37C for 30
583 minutes in a thermomixer with 1000 rpm shaking. After transposition, reactions were
584 stopped by adding EDTA to a final concentration of 40 mM. Transposed DNA fragments
585 were purified using Zymo DNA Clean and Concentrator-5 Kit (cat# D4014) and PCR
586 amplified for 5 cycles. Each PCR reaction contained 2.5 µl of 25 µM i5 primer, 2.5 µl of
587 25 µM i7 primer, 25 µl 2x NEBNext high-fidelity 2x master mix (NEB # M0541), and 20
588 µl transposed/cleaned-up DNA sample. PCR conditions were as follows: 72ºC for 5 min,
589 98ºC for 30 sec, followed by 5 cycles of [98ºC for 10 sec, 63ºC for 30 sec, 72ºC for 1
590 min] and then kept at 4ºC. PCR reactions were purified using the Zymo kit. The purified
591 ATAC libraries were quantified on an Aligent TapeStation using D5000 high sensitivity
592 tapes and mixed at an equal molar ratio. The library pool then was size-selected for
593 100-1000 bp on a 1% agarose gel. The final library pool was sequenced on Illumina
594 NextSeq2000 for a 100 bp pair-ended run to obtain 100 million reads per sample.
595
596 <u>ATAC-seq Analysis</u>
597 FASTQ files were processed using the PEPATAC (v 2.0.0) pipeline [48] against the
598 hg38 build of the human genome. Briefly, reads were trimmed of adaptors using Skewer
599 and aligned to hg38 using Bowtie2. Duplicates were removed using Samblaster. Peaks
600 were called using MACS2. Differently accessible regions were determined using
601 DESeq2 (version 1.26.0) within R Studio (version 3.6.3). *De novo* and known motif
602 enrichment analysis was performed with HOMER [49]. Changes in TF occupancy
603 between the two cell states was performed with the BaGFoot algorithm [50].

604

605 *Chromatin extraction and MNase+ExoIII-seq assay*

606 Cells were harvested at 80% confluency using a cell scraper, centrifuged at 125g for 5
607 min and washed once with cold phosphate-buffered saline. Cells were then
608 resuspended in cold RSB buffer (10 mM Tris-HCl, pH 8.0, 10 mM NaCl, 3 mM $MgCl_2$)
609 containing 0.5% Nonidet P-40, 1 mM PMSF and put on ice. The cell suspensions were
610 homogenized by 20 strokes of pestle B in a Dounce homogenizer over 30 min on ice.
611 Release nuclei were centrifuged in Sorvall X Pro centrifuge at 150g, 4ºC for 5 min,
612 nuclei pellet was resuspended in cold RSB buffer supplemented with 1 mM PMSF.

613 Before digestion, $1x10^6$ nuclei in RSB buffer with 1 mM PMSF were
614 supplemented with 2 mM $CaCl_2$ and kept at 37ºC for 5 min. 5 units of Micrococcal
615 nuclease (Nuclease S7 Micrococcal Nuclease, cat# 10107921001; Roche Applied
616 Science) with 200 units ExoIII (cat# M0206S; New England Biolabs) were added to
617 each nuclei aliquot and incubated for 10 min at 37ºC. The reaction was stopped by
618 adding EDTA to a final concentration of 5 mM. Digested nuclei were centrifuged at
619 4,600g in a Sorvall Legend Micro tabletop centrifuge, supernatant S1 was removed and
620 discarded. Pellet was resuspended in cold TE buffer, (10 mM Tris-HCl pH 8.0, 1 mM
621 EDTA), gently pipetted and incubated on ice for 10 min. After centrifugation supernatant
622 S2 was collected, pelleted material was resuspended in TE buffer, and after third
623 centrifugation supernatant S3 was collected. Supernatants 2 and 3 were analyzed on
624 1% agarose gel in TAE buffer to confirm the release of DNA fragments of various
625 length, then combined and treated with 1% SDS and 20 µg of proteinase K (New
626 England Biolabs, #P8107S). The reaction was incubated for 1 h at 55ºC. DNA was
627 extracted with phenol-chloroform-isoamyl alcohol, precipitated in 2.5 volumes of 100%

628 alcohol supplemented with 50 mM sodium-acetate and left at -80ºC for overnight.
629 Samples were centrifuged at 17,000g at a tabletop centrifuge, pellet was rinsed in 70%
630 alcohol, air dried and dissolved in TE buffer (10 mM Tris-HCl, pH 8.0, 0.2 mM EDTA).
631 Total DNA was sequenced on Illumina NextSeq2000 for a 100 bp pair-ended run to
632 obtain 300 million reads per sample.
633
634 *LC-MS to detect methylated romidepsin in culture medium*
635 Media was centrifuged 5000 × g 15 minutes to pellet any insoluble material and 50 µL of
636 supernatant removed for mass spectrometry analysis. For each, 10 10 µL was injected
637 on an Exion liquid chromatography system (SCIEX, Framingham, MA) coupled inline to
638 an X500B QTOF mass spectrometer (SCIEX, Framingham, MA) in-line with an Exion
639 liquid chromatography system (SCIEX, Framingham, MA). Each sample was separated
640 on a 2.1 x 50 mm Aeris 3.6 µm WIDEPORE XB-C8 200 Å column (Phenomenex,
641 Torrance, CA) at 0.3 mL/min using a 4 min linear gradient from 98% A (0.1% formic
642 acid) to 40% B (acetonitrile with 0.1% formic acid). Data was acquired in positive mode
643 over a mass range of 100-800 m/z with data dependent acquisition MS/MS performed
644 over the mass range of 50-750 m/z. Relative quantitation was performed from extracted
645 ion chromatogram peak areas using SCIEX OS software (SCIEX, Framingham, MA).
646
647 *Reduction of romidepsin*
648 Romidepsin was added to 1 mL of deoxygenated 50 mM Tris-HCl buffer pH 7.5 with 10
649 mM TCEP. The final romidepsin concentration was 1 mM and was incubated at 37 °C
650 for 1.5 h in the TCEP-containing, buffered solution. At 1.5 h the romidepsin, now almost

651 completely reduced, was extracted with 1X ethyl acetate. Briefly, 1mL of ethyl acetate
652 was added to the 1 mL solution of, now reduced, romidepsin. The entire solution was
653 vortexed, centrifuged briefly at 5000 x g, and then incubated at -80 °C to freeze the
654 aqueous components. The top layer of ethyl acetate does not freeze and was
655 transferred to a new vial and dried with a slow stream of nitrogen gas. The dried
656 reduced romidepsin was then reconstituted with acetonitrile.
657
658 *Synthesis of (D3)2-diemthyl-romidepsin*
659 We determined that, when reduced with TCEP as previously described, romidepsin was
660 almost completely converted to the reduced form. We therefore assumed that when
661 reconstituted with acetonitrile, the solution contains approx. 1 µmol of reduced
662 romidepsin. All reagents are added based on this estimated yield of reduced
663 romidepsin. To a solution of acetonitrile containing 1 µmol of reduced romidepsin
664 dissolved in acetonitrile, 10 µmol of N,N-Diisopropylethylamine (DIPEA) and 5 umol of
665 D3-iodomethane were added. The solution was incubated at room temperature for 2 h
666 before adding a small volume of water to quench the remaining iodomethane. The
667 solution was then dried down with a slow stream of nitrogen gas. The dried D3-
668 dimethyl-romidepsin was then reconstituted with acetonitrile and stored at -80 °C.
669
670 *Romidepsin methylation activity with purified enzyme*
671 Purified N-GST-METTL7A and -METTL7B were individually diluted to 0.2 mg/mL in KPi
672 reaction buffer (50 mM KPi pH 7.0, 20% glycerol, 150 mM NaCl, 10 mM CHAPS). The
673 diluted purified thiol methyltransferases were then added 1:2 to a solution of 9 mg/mL

674 1,2-Dimyristoyl-sn-glycero-3-phospho-rac-(1-glycerol) sodium salt (DMPG) dissolved in
675 KPi reaction buffer. The final protein concentration was 0.07 mg/mL for each protein.
676 The solutions of diluted protein were incubated on ice for 30 mins. Small volumes of
677 diluted METTL7A and METTL7B were then aliquoted into separate vials and boiled for 5
678 min to inactivate the enzymes. A small volume of reduced romidepsin was deposited
679 into relevant wells of a 96-well reaction plate. The acetonitrile solvent was removed by
680 placing the plate in a vacuum chamber and pulling a vacuum for several minutes. The
681 diluted proteins were added to the plate wells containing dried reduced romidepsin.
682 Vehicle control was then added to relevant wells containing the diluted thiol
683 methyltransferases. The well plate was allowed to shake at 625 rpm on a plate shaker
684 for 5 min. Finally, SAM or a vehicle control of liquid chromatography-grade water was
685 added to the appropriate wells to initiate the reaction. The final concentration of protein
686 was 0.06 mg/mL and the final concentration of SAM was 500 μM. The estimated final
687 concentration of reduced romidepsin was approx. 500 μM. After SAM was added to
688 initiate the reaction, the samples were incubated at 37 °C for 2 h. After 2 h, ice-cold
689 acetonitrile containing the (D3)2-dimethyl-romidepsin internal standard was added to
690 precipitate salts and proteins at a ratio of 3:7 (reaction volume:MeCN). The plate was
691 centrifuged at 5000 x g for 20 min and then the supernatant from each well was
692 transferred to a new well in a 96-well plate for LC-MS analysis.
693
694 Samples were analyzed with a Waters Xevo TQS mass spectrometer paired with a
695 Waters Acquity LC using a 2.1 × 50 mm Waters 1.7 μm C18 column and 0.2% acetic
696 acid in water (Buffer A) and 0.2% acetic acid in MeCN (Buffer B). Consistent elution of

697 romidepsin analytes was achieved with the following gradient: solvent B held at 5% from
698 0 to 0.15 min, then increased to 95% from 0.15 to 5 min, followed by re-equilibration to
699 the starting conditions for another 2 min for a total run time of 7 min. Flow rate was held
700 constant at 0.35 mL/min. The transition used to monitor for the early monomethyl
701 metabolites was 557.74> 255.
702
703 *Immunohistochemistry*
704 Serial sections from normal tissue microarrays (BCN921 and BN1021) were
705 obtained from tissuearray.com (Derwood, MD). Slides were immunolabeled for METTLA
706 and METTLB according to the conditions in Supplemental Table S6. Serial sections
707 were also stained with a negative control protocol in which primary antibody was
708 replaced by nonclonal antibody from the same species and of the same isotypes
709 (isotype controls). Positive controls included cell pellet slides with known expression of
710 METTL7A (7A 1-2, 7A 1-4) and METTL7B (7B 1-3, 7B 2-2). Slides were analyzed and
711 each tissue was manually evaluated for positive staining along with negative controls;
712 positive cell types were listed and assigned a semi-quantitative grade for positivity
713 (minimal, mild, moderate, or marked; 1+, 2+, 3+, 4+). Slides were also digitalized and
714 analyzed using QuPath (v 0.3.2) [51]. Digital image analysis included identifying stain
715 vectors, de-arraying tissue microarrays, defining regions of interest, cell detection, and
716 quantifying chromogenic immunohistochemistry staining. Following automated TMA grid
717 detection, manual pathologist review was performed to exclude spots or regions of
718 spots that were non-assessable, non-tumor containing, or obscured by artifact.
719

720 **Figure Legends**

721

722 **Fig. 1. MCF-7 DpVp300 cells are selectively resistant to romidepsin.**

723 (A) Three-day cytotoxicity assays were performed on MCF-7 cells (black circles) and
724 MCF-7 DpVp300 cells (blue triangles) with the histone deacetylase inhibitors
725 romidepsin, belinostat, panibinostat and vorinostat.

726 (B) MCF-7 and MCF-7 DpVp300 cells were plated and allowed to attach overnight.
727 Cells were subsequently treated with belinostat (5 μM), romidepsin (10 ng/ml),
728 panobinostat (5 μM), or vorinostat (5 μM) for 24 h after which protein was extracted and
729 subjected to immunoblot analysis. Membranes were incubated with antibodies to pan
730 acetylated histone H3 (AcH3), total histone H3 (total H3), p21 or actin. One of three
731 independent experiments is shown.

732 (C) MCF-7 and MCF-7 DpVp300 cells were plated and allowed to attach overnight after
733 which cells were exposed to belinostat (5 μM), romidepsin (10 ng/ml), panobinostat (5
734 μM), or vorinostat (5 μM) for 24 h. Cells were subsequently analyzed by flow cytometry
735 and the percentage of cells in each phase of the cell cycle was determined using ModFit
736 LT v 5.0. The graph was generated from data compiled from three independent
737 experiments. Error bars are standard deviation.

738 (D). MCF-7 and MCF-7 DpVp300 cells were plated and allowed to attach overnight after
739 which cells were exposed to increasing concentrations of romidepsin for 24 h. After
740 harvesting cells and subjecting extracted protein to immunoblot analysis, proteins were
741 probed with antibodies as described in (B). One of three independent experiments is
742 shown.

743

744 **Fig. 2. RNA Seq and ATAC Seq analysis of MCF-7 and MCF-7 DpVp300 cells**.

745 (A) Volcano plot depicting steady state fold change in mRNA levels between MCF-7 and
746 MCF-7 DpVp300 (left) and HuT78 and HuT78 DpVp50 (right). Changes in gene
747 expression were determined with DEseq2. The drug efflux gene *ABCB1* and *METTL7A*
748 are indicated with a red line

749 (B) Scatterplot depicting the log2 fold change of transcripts in MCF-7 and MCF-7
750 DpVp300 compared to the log2 fold change in HuT78 and HuT78 DpVp50 cells. A log2
751 fold change of 5 is indicated on the x and y-axis with a dashed line. *METTL7A* is
752 indicated with a red line.

753 (C) Immunoblot of METTL7A in the MCF-7 and HuT78 resistance models.

754 (D) Volcano plot depicting the fold change of differentially open regions in MCF7 cells
755 (left) and Hut78 cells (right) identified with PEPATAC.

756 (E) Heatmap depicting changes in the differentially open regions in MCF-7, MCF-7
757 DpVp300, HuT78 and HuT78 DpVp50 cells.

758 (F) Box plot showing log2 fold change in mRNA levels for genes linked to differentially
759 open region that gain or lose accessibility in DpVp cells. Genes linked to differentially
760 open regions with both gain and loss of accessibility are excluded.

761 (G) Differentially open regions at the genomic locus of METTL7A in MCF-7, MCF-7
762 DpVp300, HuT78, and HuT78 DpVp50 cells.

763

764 **Fig. 3. METTL7A overexpression confers resistance to thiol-based HDACIs in the**
765 **MCF-7 DpVp300 line**

766 (A) Three-day cytotoxicity assays were performed on MCF-7 cells (black circles) and
767 MCF-7 DpVp300 cells (blue triangles) with KD-5170, largazole, NCH-51, and OKI-005.
768 (B) MCF-7 and MCF-7 DpVp300 cells were plated and allowed to attach overnight.
769 Cells were subsequently treated with romidepsin (10 ng/ml), KD-5170 (10 μM),
770 largazole (250 nM), NCH-51 (25 μM), or OKI-005 (500 nM) for 24 h after which protein
771 was extracted and subjected to immunoblot. Blots were incubated with antibodies to
772 pan acetylated histone H3 (AcH3), total histone H3 (total H3), p21 or actin. Results from
773 one of three independent experiments are shown.
774
775 **Fig. 4. Deletion of METTL7A restores sensitivity to thiol-based HDACIs in MCF-7**
776 **DpVp300 cells**
777 (A) MCF-7 and MCF-7 DpVp300 cells, as well as knockout clones (7A KO B1 and 7A
778 KO B3) and partial knockdown clone 7A KO B4 were plated and allowed to attach
779 overnight. Cells were subsequently left untreated or treated with romidepsin (10 ng/ml)
780 for 24 h. After harvesting cells and subjecting extracted protein to PAGE, proteins were
781 transferred to nitrocellulose that was probed with METTL7A antibody as well as pan
782 acetylated histone H3 (AcH3), total histone H3 (total H3), p21 or actin antibodies.
783 (B) Three-day cytotoxicity assays were performed with romidepsin, KD-5170, largazole,
784 NCH-51, OKI-005 and vorinostat on MCF-7 cells (black circles), MCF-7 DpVp300 cells
785 (blue triangles), 7A KO B1 cells (open black squares), 7A KO B3 (inverted green
786 triangles) and 7A KO B4 (purple diamonds).
787 (C) MCF-7, MCF-7 DpVp300 and 7A KO B1 cells were plated and allowed to attach
788 overnight. Cells were subsequently treated with romidepsin (10 ng/ml), KD-5170 (10

789 μM), largazole (250 nM), NCH-51 (25 μM), or OKI-005 (500 nM) for 24 h after which
790 protein was extracted and subjected to PAGE. Proteins were transferred to
791 nitrocellulose membranes and blots were incubated with antibodies to pan acetylated
792 histone H3 (AcH3), total histone H3 (total H3), p21 or actin. Results from one of three
793 independent experiments is shown.
794 (D) MCF-7, MCF-7 DpVp300 and 7A KO B1 cells were plated and allowed to attach
795 overnight after which cells were exposed to belinostat (5 μM), romidepsin (10 ng/ml),
796 panobinostat (5 μM), or vorinostat (5 μM) for 24 h. Cell cycle analysis was subsequently
797 performed and the percentage of cells in each phase was determined using ModFit LT v
798 5.0. The graph was generated from data compiled from three independent experiments.
799 Error bars indicate standard deviation.
800
801 **Fig. 5. METTL7A and METTL7B overexpression confers varying levels of**
802 **resistance to thiol-based HDACis**.
803 (A) HEK293 cells were transfected with empty vector (vector) or with vector encoding
804 METTL7A (clones 7A 1-2 and 7A 1-4) or METTL7B (clones 7B 1-3 and 7B 2-2).
805 Proteins were extracted and subjected to immunoblot. The blots were probed with
806 antibodies to METTL7A, METTL7B or actin.
807 (B) Three-day cytoptoxicity assays were performed with romidepsin, KD-5170,
808 largazole, or OKI-005 on empty vector (vector) cells (black circles), 7A 1-2 cells (blue
809 triangles), 7A 1-4 cells (open black squares), 7B 1-3 (inverted green triangles) and 7B
810 2-2 (purple diamonds).

811 (C) Empty vector (vector) cells, 7A 1-2 cells, 7A 1-4 cells, 7B 1-3 cells, and 7B 2-2 cells
812 were plated and treated with romidepsin (10 ng/ml), KD-5170 (10 μM), largazole (250
813 nM), NCH-51 (25 μM), or OKI-005 (500 nM) for 24 h after which protein was extracted
814 and subjected to PAGE. Proteins were transferred to nitrocellulose membranes and
815 blots were incubated with antibodies to pan acetylated histone H3 (AcH3), total histone
816 H3 (total H3), p21 or actin. Results from one of three independent experiments is
817 shown.
818 (D) Empty vector (vector) cells, 7A 1-2 cells, 7A 1-4 cells, 7B 1-3 cells, and 7B 2-2 cells
819 were plated and treated with romidepsin (10 ng/ml), KD-5170 (10 μM), largazole (250
820 nM), NCH-51 (25 μM), or OKI-005 (500 nM) for 24 h after which cell cycle analysis was
821 performed. The percentage of cells in each phase was determined using ModFit LT v
822 5.0. The graph was generated from data compiled from 3 independent experiments.
823 Error bars indicate standard deviation.
824
825 **Figure 6. METTL7A methylation of romidepsin *in vitro***
826 (A) Measurement of dimethylated romidepsin by LC-MS/MS in cell culture media
827 following 24 h of incubation with MCF-7, MCF-7 DpVp300, 7A KO B1 and 7A KO B3
828 cells.
829 (B) Measurement of methylated romidepsin with METTL7A and METTL7B in a cell-free
830 system. Methylation reactions were carried out with recombinant enzyme and the
831 amount of methylated product was measured by LC-MS/MS. Omission of the methyl
832 donor SAM, and boiling the enzyme were used as controls.

833 (C) Three-day cytotoxicity assays were performed with NCH-51 on empty vector
834 (vector) cells (black circles), empty vector cells with DCMB (blue triangles) 7A 1-2 cells
835 (open black squares) 7A 1-2 cells with DCMB (inverted green triangles) 7A 1-4 cells
836 (purple diamonds), and 7A 1-2 cells with DCMB (open black circles).
837 (D) Three-day cytotoxicity assays were performed with NCH-51 on empty vector
838 (vector) cells (black circles), empty vector cells with DCMB (blue triangles) 7B 1-3 cells
839 (open black squares) 7B 1-3 cells with DCMB (inverted green triangles) 7B 2-2 cells
840 (purple diamonds), and 7B 2-2 cells with DCMB (open black circles).
841
842 **Figure 7: Normal Tissue Expression and proposed model**
843 Normal tissue expression of METTL7A and METTL7B. A strong cytoplasmic pattern is
844 observed in hepatocytes (A and B), distinct regions of the nephron (C and D), small
845 intestinal enterocytes (E and F), and breast epithelium (G and H). Arrows and asterisks
846 indicate distinct METTL7A and METTL7B expression patterns in renal tubules on serial
847 sections. Scale bars represent 20 μm (A and B), 100 μm (C and D), and 50 μm (E, F, G,
848 and H). (I) Proposed model of drug resistance through activity of METTL7A.
849
850 **Supplemental Fig. S1. MCF-7 DpVp300 are selectively resistant to romidepsin and**
851 **do not overexpress P-gp.**
852 (A) MCF-7 and MCF-7 DpVp300 cells were plated and treated with the noted
853 concentrations of HDACI for 24 h, after which cells were harvested and cell cycle
854 analysis was performed as detailed in the materials and methods.

855 (B) MCF-7, MCF-7 DpVp300, pcDNA, and MDR-19 cells were trypsinized and
856 incubated with isotype control antibody (solid line) or UIC-2 antibody (dashed line) and
857 fluorescence was measured on a FACSCanto flow cytometer.
858 (C) Three-day cytotoxicity assays were performed with romidepsin on pcDNA cells
859 (black circles) and MDR-19 (blue triangles). Results from one of three experiments is
860 shown.
861
862 **Supplemental Fig. S2. RNA Seq and ATAC Seq analysis of MCF-7, MCF-7**
863 **DpVp300, HuT78 and HuT78 DpVp50 cells.**
864 (A) Gene ontology (GO)-Term analysis of up- and down-regulated genes from RNA-
865 seq analysis in the MCF-7 and HuT-78 romidpesin resistance models. (B) *De novo* motif
866 analysis of open DORs or closed DORs in the MCF-7 and Hut-78 romidepsin resistance
867 models. (C) Histogram representation of short nucleosome (80-140bp) density in MCF-7
868 and MCF-7 DpVp300 cells. METTL7B is shown as example of a gene that does not
869 change. (D) Histogram representing misincorporation frequency in RNA sequencing
870 experiments in MCF-7 DpVp300 and HuT78 DpVp50 cells. Red represents A to G
871 changes, black all other changes.
872
873 **Supplemental Fig. S3. Thiol-based HDACIs induce cell cycle changes after**
874 **deletion of METTL7A in MCF-7 DpVp300 cells.**
875 MCF-7, MCF-7 DpVp300, 7A KO B1, 7A KO B3 and 7A KO B4 cells were plated and
876 treated with the noted concentrations of HDACi for 24 h, after which cells were
877 harvested and cell cycle analysis was performed as detailed in Materials and Methods.

878

879 **Supplemental Fig. S4. METTL7A overexpression prevents cell cycle changes**

880 **mediated by thiol-based HDACis**

881 Vector, 7A 1-2, 7A 1-4, 7B 1-3 and 7B 2-2 cells were plated and treated with the noted

882 concentrations of HDACI for 24 h, after which cells were harvested and cell cycle

883 analysis was performed as detailed in Materials and Methods.

884

885 **REFERENCES**
886
887 1. Bates SE. Epigenetic Therapies for Cancer. N Engl J Med. 2020;383(7):650-63. Epub
888 2020/08/14. doi: 10.1056/NEJMra1805035. PubMed PMID: 32786190.
889 2. Piekarz RL, Sackett DL, Bates SE. Histone deacetylase inhibitors and demethylating
890 agents: clinical development of histone deacetylase inhibitors for cancer therapy. Cancer J.
891 2007;13(1):30-9. PubMed PMID: 17464244.
892 3. Richon VM. Targeting histone deacetylases: development of vorinostat for the
893 treatment of cancer. Epigenomics. 2010;2(3):457-65. Epub 2010/06/01. doi: 10.2217/epi.10.20.
894 PubMed PMID: 22121904.
895 4. Robey RW, Chakraborty AR, Basseville A, Luchenko V, Bahr J, Zhan Z, et al. Histone
896 deacetylase inhibitors: emerging mechanisms of resistance. Mol Pharm. 2011;8(6):2021-31. doi:
897 10.1021/mp200329f. PubMed PMID: 21899343; PubMed Central PMCID: PMCPMC3230675.
898 5. Duvic M, Talpur R, Ni X, Zhang C, Hazarika P, Kelly C, et al. Phase 2 trial of oral vorinostat
899 (suberoylanilide hydroxamic acid, SAHA) for refractory cutaneous T-cell lymphoma (CTCL).
900 Blood. 2007;109(1):31-9. PubMed PMID: 16960145.
901 6. Olsen E, Kim Y, Kuzel T, Pacheco T, Foss F, Parker S, et al. Phase IIb multicenter trial of
902 vorinostat in patients with persistent, progressive, or treatment refractory cutaneous T-cell
903 lymphoma. J Clin Oncol. 2007;25(21):3109-15. PubMed PMID: 17577020.
904 7. Whittaker SJ, Demierre MF, Kim EJ, Rook AH, Lerner A, Duvic M, et al. Final results from
905 a multicenter, international, pivotal study of romidepsin in refractory cutaneous T-cell
906 lymphoma. J Clin Oncol. 2010;28(29):4485-91. doi: JCO.2010.28.9066 [pii]
907 10.1200/JCO.2010.28.9066. PubMed PMID: 20697094.
908 8. Piekarz R, Frye R, Turner M, Wright J, Allen S, Kirschbaum M, et al. Phase II multi-
909 institutional trial of the histone deacetylase inhibitor romidepsin as monotherapy for patients
910 with cutaneous T-cell lymphoma. J Clin Oncol. 2009;27(32):5410-7. PubMed PMID: 19826128.
911 9. O'Connor OA, Horwitz S, Masszi T, Van Hoof A, Brown P, Doorduijn J, et al. Belinostat in
912 Patients With Relapsed or Refractory Peripheral T-Cell Lymphoma: Results of the Pivotal Phase
913 II BELIEF (CLN-19) Study. J Clin Oncol. 2015;33(23):2492-9. Epub 2015/06/22. doi:
914 10.1200/JCO.2014.59.2782. PubMed PMID: 26101246; PubMed Central PMCID:
915 PMCPMC5087312.
916 10. Shi Y, Dong M, Hong X, Zhang W, Feng J, Zhu J, et al. Results from a multicenter, open-
917 label, pivotal phase II study of chidamide in relapsed or refractory peripheral T-cell lymphoma.
918 Ann Oncol. 2015;26(8):1766-71. Epub 2015/06/25. doi: 10.1093/annonc/mdv237. PubMed
919 PMID: 26105599.
920 11. Furumai R, Matsuyama A, Kobashi N, Lee KH, Nishiyama M, Nakajima H, et al. FK228
921 (depsipeptide) as a natural prodrug that inhibits class I histone deacetylases. Cancer Res.
922 2002;62(17):4916-21.
923 12. Lee JS, Paull K, Alvarez M, Hose C, Monks A, Grever M, et al. Rhodamine efflux patterns
924 predict P-glycoprotein substrates in the National Cancer Institute Drug Screen. Mol Pharmacol.
925 1994;46:627-38.
926 13. Robey RW, Zhan Z, Piekarz RL, Kayastha GL, Fojo T, Bates SE. Increased MDR1 expression
927 in normal and malignant peripheral blood mononuclear cells obtained from patients receiving

928 depsipeptide (FR901228, FK228, NSC630176). Clin Cancer Res. 2006;12(5):1547-55. PubMed
929 PMID: 16533780.
930 14. Tabe Y, Konopleva M, Contractor R, Munsell M, Schober W, Jin L, et al. Up-regulation of
931 MDR1 and induction of doxorubicin resistance by histone deacetylase inhibitor depsipeptide
932 (FK228) and ATRA in acute promyelocytic leukemia cells. Blood. 2006;107(4):1546-54. PubMed
933 PMID: 16223781.
934 15. Xiao JJ, Foraker AB, Swaan PW, Liu S, Huang Y, Dai Z, et al. Efflux of depsipeptide FK228
935 (FR901228, NSC-630176) is mediated by P-glycoprotein and multidrug resistance-associated
936 protein 1. J Pharmacol Exp Ther. 2005;313(1):268-76.
937 16. Yamada H, Arakawa Y, Saito S, Agawa M, Kano Y, Horiguchi-Yamada J. Depsipeptide-
938 resistant KU812 cells show reversible P-glycoprotein expression, hyper-acetylated histones, and
939 modulated gene expression profile. Leuk Res. 2006;30(6):723-34. PubMed PMID: 16260035.
940 17. Bates S, Zhan Z, Steadman K, Obrzut T, Luchenko V, Frye R, et al. Laboratory correlates
941 for a phase II trial of romidepsin in cutaneous and peripheral T-cell lymphoma. Br J Haematol.
942 2010;148(2):256-67. PubMed PMID: 19874311.
943 18. Chakraborty AR, Robey RW, Luchenko VL, Zhan Z, Piekarz RL, Gillet JP, et al. MAPK
944 pathway activation leads to Bim loss and histone deacetylase inhibitor resistance: rationale to
945 combine romidepsin with an MEK inhibitor. Blood. 2013;121(20):4115-25. doi: 10.1182/blood-
946 2012-08-449140. PubMed PMID: 23532732.
947 19. Richon VM, Sandhoff TW, Rifkind RA, Marks PA. Histone deacetylase inhibitor selectively
948 induces p21WAF1 expression and gene-associated histone acetylation. Proc Natl Acad Sci U S A.
949 2000;97(18):10014-9. PubMed PMID: 10954755.
950 20. Sandor V, Robbins AR, Robey R, Myers T, Sausville E, Bates SE, et al. FR901228 causes
951 mitotic arrest but does not alter microtubule polymerization. Anticancer Drugs. 2000;11(6):445-
952 54.
953 21. Landreville S, Agapova OA, Matatall KA, Kneass ZT, Onken MD, Lee RS, et al. Histone
954 deacetylase inhibitors induce growth arrest and differentiation in uveal melanoma. Clin Cancer
955 Res. 2012;18(2):408-16. Epub 2011/10/28. doi: 10.1158/1078-0432.CCR-11-0946. PubMed
956 PMID: 22038994; PubMed Central PMCID: PMCPMC3261307.
957 22. Bernhart E, Stuendl N, Kaltenegger H, Windpassinger C, Donohue N, Leithner A, et al.
958 Histone deacetylase inhibitors vorinostat and panobinostat induce G1 cell cycle arrest and
959 apoptosis in multidrug resistant sarcoma cell lines. Oncotarget. 2017;8(44):77254-67. Epub
960 2017/11/05. doi: 10.18632/oncotarget.20460. PubMed PMID: 29100385; PubMed Central
961 PMCID: PMCPMC5652778.
962 23. Piekarz RL, Robey RW, Zhan Z, Kayastha G, Sayah A, Abdeldaim AH, et al. T-cell
963 lymphoma as a model for the use of histone deacetylase inhibitors in cancer therapy: impact of
964 depsipeptide on molecular markers, therapeutic targets, and mechanisms of resistance. Blood.
965 2004;103(12):4636-43.
966 24. Yi X, Liu J, Wu P, Gong Y, Xu X, Li W. The key microRNA on lipid droplet formation during
967 adipogenesis from human mesenchymal stem cells. J Cell Physiol. 2020;235(1):328-38. Epub
968 2019/06/19. doi: 10.1002/jcp.28972. PubMed PMID: 31210354.
969 25. Maldonato BJ, Russell DA, Totah RA. Human METTL7B is an alkyl thiol methyltransferase
970 that metabolizes hydrogen sulfide and captopril. Sci Rep. 2021;11(1):4857. Epub 2021/03/03.

971 doi: 10.1038/s41598-021-84218-5. PubMed PMID: 33649426; PubMed Central PMCID:
972 PMCPMC7921093.
973 26. Liu Y, Salvador LA, Byeon S, Ying Y, Kwan JC, Law BK, et al. Anticolon cancer activity of
974 largazole, a marine-derived tunable histone deacetylase inhibitor. J Pharmacol Exp Ther.
975 2010;335(2):351-61. Epub 2010/08/27. doi: 10.1124/jpet.110.172387. PubMed PMID:
976 20739454; PubMed Central PMCID: PMCPMC2967399.
977 27. Wang X, Waschke BC, Woolaver RA, Chen Z, Zhang G, Piscopio AD, et al. Histone
978 Deacetylase Inhibition Sensitizes PD1 Blockade-Resistant B-cell Lymphomas. Cancer Immunol
979 Res. 2019;7(8):1318-31. Epub 2019/06/27. doi: 10.1158/2326-6066.CIR-18-0875. PubMed
980 PMID: 31235619; PubMed Central PMCID: PMCPMC6679731.
981 28. Hassig CA, Symons KT, Guo X, Nguyen PM, Annable T, Wash PL, et al. KD5170, a novel
982 mercaptoketone-based histone deacetylase inhibitor that exhibits broad spectrum antitumor
983 activity in vitro and in vivo. Mol Cancer Ther. 2008;7(5):1054-65. Epub 2008/05/17. doi:
984 10.1158/1535-7163.MCT-07-2347. PubMed PMID: 18483295.
985 29. Suzuki T, Nagano Y, Kouketsu A, Matsuura A, Maruyama S, Kurotaki M, et al. Novel
986 inhibitors of human histone deacetylases: design, synthesis, enzyme inhibition, and cancer cell
987 growth inhibition of SAHA-based non-hydroxamates. J Med Chem. 2005;48(4):1019-32. Epub
988 2005/02/18. doi: 10.1021/jm049207j. PubMed PMID: 15715470.
989 30. Russell DA, Chau MK, Shi Y, Maldonato BJ, Totah RA. METTL7A and METTL7B are
990 responsible for S-thiol methyl transferase activity in liver. bioRxiv.
991 2022:2022.10.12.511968. doi: 10.1101/2022.10.12.511968.
992 31. Glozak M, Seto E. Histone deacetylases and cancer. Oncogene. 2007;26(37):5420-32.
993 PubMed PMID: 17694083.
994 32. Piekarz RL, Frye R, Prince HM, Kirschbaum MH, Zain J, Allen SL, et al. Phase 2 trial of
995 romidepsin in patients with peripheral T-cell lymphoma. Blood. 2011;117(22):5827-34. doi:
996 10.1182/blood-2010-10-312603. PubMed PMID: 21355097; PubMed Central PMCID:
997 PMCPMC3112033.
998 33. Qi L, Song Y, Chan THM, Yang H, Lin CH, Tay DJT, et al. An RNA editing/dsRNA binding-
999 independent gene regulatory mechanism of ADARs and its clinical implication in cancer. Nucleic
1000 Acids Res. 2017;45(18):10436-51. Epub 2017/10/07. doi: 10.1093/nar/gkx667. PubMed PMID:
1001 28985428; PubMed Central PMCID: PMCPMC5737565.
1002 34. Zhou S, Shen Y, Zheng M, Wang L, Che R, Hu W, et al. DNA methylation of METTL7A
1003 gene body regulates its transcriptional level in thyroid cancer. Oncotarget. 2017;8(21):34652-
1004 60. Epub 2017/04/19. doi: 10.18632/oncotarget.16147. PubMed PMID: 28416772; PubMed
1005 Central PMCID: PMCPMC5470999.
1006 35. Valdez BC, Brammer JE, Li Y, Murray D, Liu Y, Hosing C, et al. Romidepsin targets
1007 multiple survival signaling pathways in malignant T cells. Blood Cancer J. 2015;5:e357. Epub
1008 2015/10/17. doi: 10.1038/bcj.2015.83. PubMed PMID: 26473529; PubMed Central PMCID:
1009 PMCPMC4635192.
1010 36. Arzenani MK, Zade AE, Ming Y, Vijverberg SJ, Zhang Z, Khan Z, et al. Genomic DNA
1011 hypomethylation by histone deacetylase inhibition implicates DNMT1 nuclear dynamics. Mol
1012 Cell Biol. 2011;31(19):4119-28. Epub 2011/07/28. doi: 10.1128/MCB.01304-10. PubMed PMID:
1013 21791605; PubMed Central PMCID: PMCPMC3187370.

1014 37. Sarkar S, Abujamra AL, Loew JE, Forman LW, Perrine SP, Faller DV. Histone deacetylase
1015 inhibitors reverse CpG methylation by regulating DNMT1 through ERK signaling. Anticancer Res.
1016 2011;31(9):2723-32. PubMed PMID: 21868513.
1017 38. Jun F, Peng Z, Zhang Y, Shi D. Quantitative proteomic analysis identifies novel regulators
1018 of methotrexate resistance in choriocarcinoma. Gynecol Oncol. 2020. Epub 2020/01/21. doi:
1019 10.1016/j.ygyno.2020.01.013. PubMed PMID: 31955862.
1020 39. Song H, Liu D, Wang L, Liu K, Chen C, Wang L, et al. Methyltransferase like 7B is a
1021 potential therapeutic target for reversing EGFR-TKIs resistance in lung adenocarcinoma. Mol
1022 Cancer. 2022;21(1):43. Epub 2022/02/12. doi: 10.1186/s12943-022-01519-7. PubMed PMID:
1023 35144642; PubMed Central PMCID: PMCPMC8830004.
1024 40. Wang Z, He J, Bach DH, Huang YH, Li Z, Liu H, et al. Induction of m(6)A methylation in
1025 adipocyte exosomal LncRNAs mediates myeloma drug resistance. J Exp Clin Cancer Res.
1026 2022;41(1):4. Epub 2022/01/05. doi: 10.1186/s13046-021-02209-w. PubMed PMID: 34980213;
1027 PubMed Central PMCID: PMCPMC8722039.
1028 41. Lee E, Kim JY, Kim TK, Park SY, Im GI. Methyltransferase-like protein 7A (METTL7A)
1029 promotes cell survival and osteogenic differentiation under metabolic stress. Cell Death Discov.
1030 2021;7(1):154. Epub 2021/07/07. doi: 10.1038/s41420-021-00555-4. PubMed PMID: 34226523;
1031 PubMed Central PMCID: PMCPMC8257615.
1032 42. Biddy BA, Kong W, Kamimoto K, Guo C, Waye SE, Sun T, et al. Single-cell mapping of
1033 lineage and identity in direct reprogramming. Nature. 2018;564(7735):219-24. Epub
1034 2018/12/07. doi: 10.1038/s41586-018-0744-4. PubMed PMID: 30518857; PubMed Central
1035 PMCID: PMCPMC6635140.
1036 43. Otterson GA, Hodgson L, Pang H, Vokes EE, B CaLG. Phase II study of the histone
1037 deacetylase inhibitor Romidepsin in relapsed small cell lung cancer (Cancer and Leukemia
1038 Group B 30304). J Thorac Oncol. 2010;5(10):1644-8. doi: 01243894-201010000-00024 [pii]
1039 10.1097/JTO.0b013e3181ec1713. PubMed PMID: 20871263.
1040 44. Whitehead R, Rankin C, Hoff P, Gold P, Billingsley K, Chapman R, et al. Phase II trial of
1041 romidepsin (NSC-630176) in previously treated colorectal cancer patients with advanced
1042 disease: a Southwest Oncology Group study (S0336). Invest New Drugs. 2009;27(5):469-75.
1043 PubMed PMID: 18941712.
1044 45. Stadler WM, Margolin K, Ferber S, McCulloch W, Thompson JA. A phase II study of
1045 depsipeptide in refractory metastatic renal cell cancer. Clinical Genitourinary Cancer.
1046 2006;5(1):57-60. PubMed PMID: ISI:000242527000007.
1047 46. Molife L, Attard G, Fong P, Karavasilis V, Reid A, Patterson S, et al. Phase II, two-stage,
1048 single-arm trial of the histone deacetylase inhibitor (HDACi) romidepsin in metastatic
1049 castration-resistant prostate cancer (CRPC). Ann Oncol. 2010;21(1):109-13. PubMed PMID:
1050 19608618.
1051 47. Corces MR, Trevino AE, Hamilton EG, Greenside PG, Sinnott-Armstrong NA, Vesuna S, et
1052 al. An improved ATAC-seq protocol reduces background and enables interrogation of frozen
1053 tissues. Nat Methods. 2017;14(10):959-62. Epub 2017/08/28. doi: 10.1038/nmeth.4396.
1054 PubMed PMID: 28846090; PubMed Central PMCID: PMCPMC5623106.
1055 48. Smith JP, Corces MR, Xu J, Reuter VP, Chang HY, Sheffield NC. PEPATAC: an optimized
1056 pipeline for ATAC-seq data analysis with serial alignments. NAR Genom Bioinform.

1057 2021;3(4):lqab101. Epub 2021/12/04. doi: 10.1093/nargab/lqab101. PubMed PMID: 34859208;
1058 PubMed Central PMCID: PMCPMC8632735.
1059 49. Heinz S, Benner C, Spann N, Bertolino E, Lin YC, Laslo P, et al. Simple combinations of
1060 lineage-determining transcription factors prime cis-regulatory elements required for
1061 macrophage and B cell identities. Mol Cell. 2010;38(4):576-89. Epub 2010/06/02. doi:
1062 10.1016/j.molcel.2010.05.004. PubMed PMID: 20513432; PubMed Central PMCID:
1063 PMCPMC2898526.
1064 50. Baek S, Goldstein I, Hager GL. Bivariate Genomic Footprinting Detects Changes in
1065 Transcription Factor Activity. Cell Rep. 2017;19(8):1710-22. Epub 2017/05/26. doi:
1066 10.1016/j.celrep.2017.05.003. PubMed PMID: 28538187; PubMed Central PMCID:
1067 PMCPMC5530758.
1068 51. Bankhead P, Loughrey MB, Fernandez JA, Dombrowski Y, McArt DG, Dunne PD, et al.
1069 QuPath: Open source software for digital pathology image analysis. Sci Rep. 2017;7(1):16878.
1070 Epub 2017/12/06. doi: 10.1038/s41598-017-17204-5. PubMed PMID: 29203879; PubMed
1071 Central PMCID: PMCPMC5715110.
1072

Figure 1

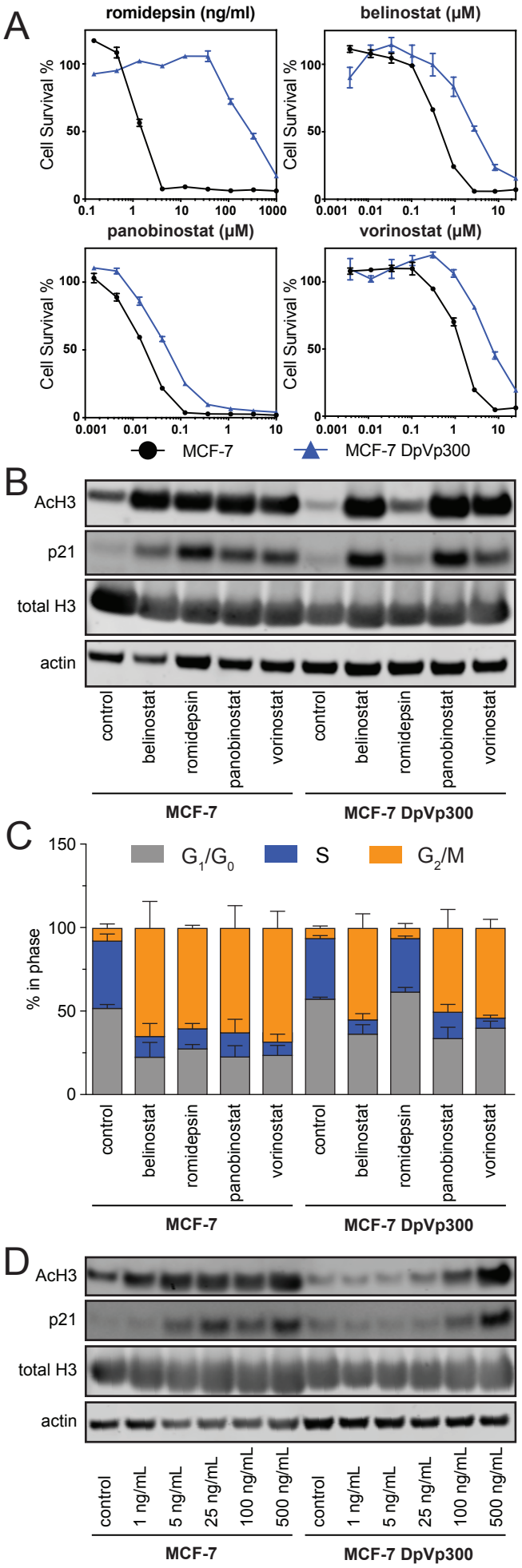
A
romidepsin (ng/ml)
belinostat (μM)
panobinostat (μM)
vorinostat (μM)
Cell Survival %
MCF-7
MCF-7 DpVp300
B
AcH3
p21
total H3
actin
control
belinostat
romidepsin
panobinostat
vorinostat
MCF-7
MCF-7 DpVp300
C
G1/G0
S
G2/M
% in phase
D
1 ng/mL
5 ng/mL
25 ng/mL
100 ng/mL
500 ng/mL

Figure 2

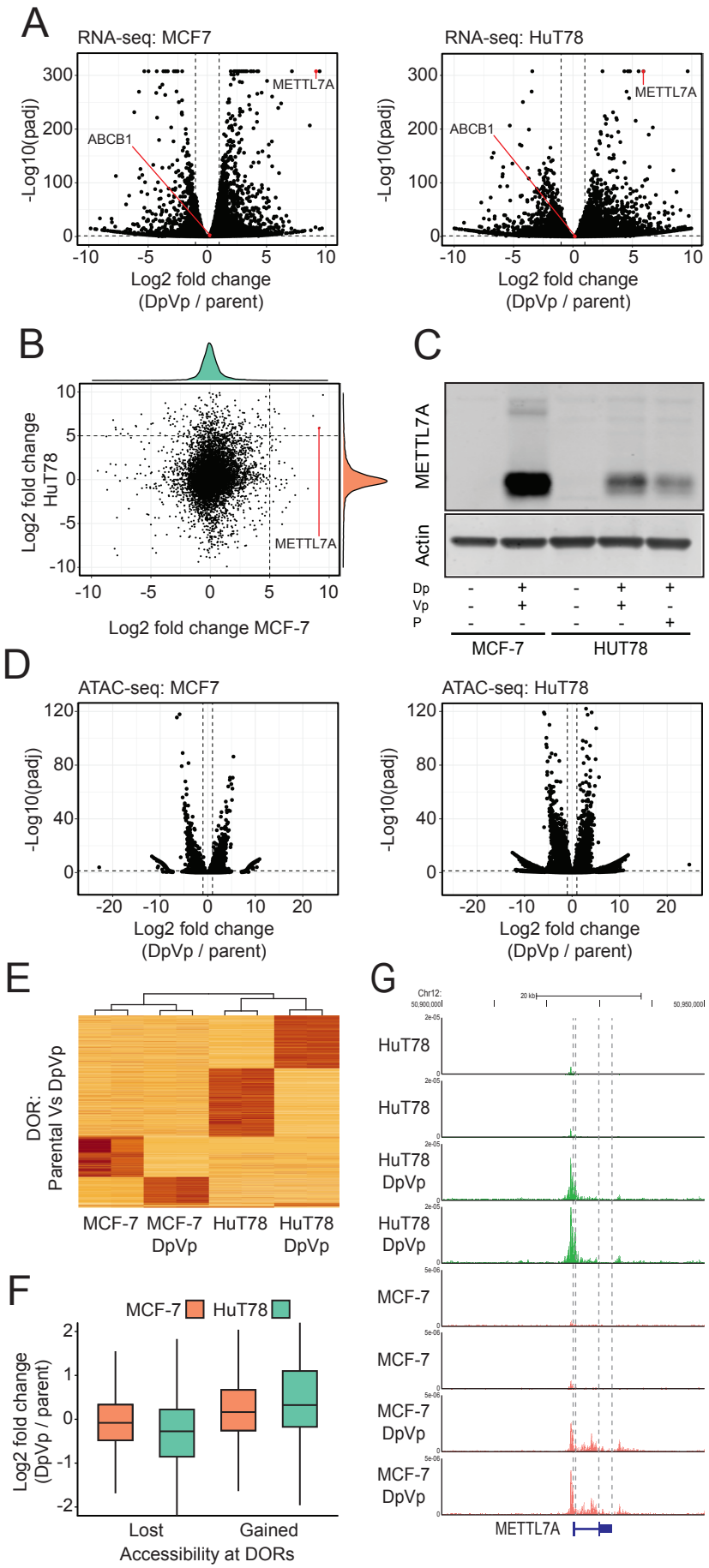
A
RNA-seq: MCF7
RNA-seq: HuT78
-Log10(padj)
Log2 fold change
(DpVp / parent)
METTL7A
ABCB1
B
Log2 fold change HuT78
Log2 fold change MCF-7
C
METTL7A
Actin
Dp
Vp
P
MCF-7
HUT78
D
ATAC-seq: MCF7
ATAC-seq: HuT78
E
DOR:
Parental Vs DpVp
MCF-7
MCF-7 DpVp
HuT78
HuT78 DpVp
F
MCF-7
HuT78
Log2 fold change
(DpVp / parent)
Lost
Gained
Accessibility at DORs
G
Chr12:
HuT78
HuT78 DpVp
MCF-7
MCF-7 DpVp
METTL7A

Figure 3

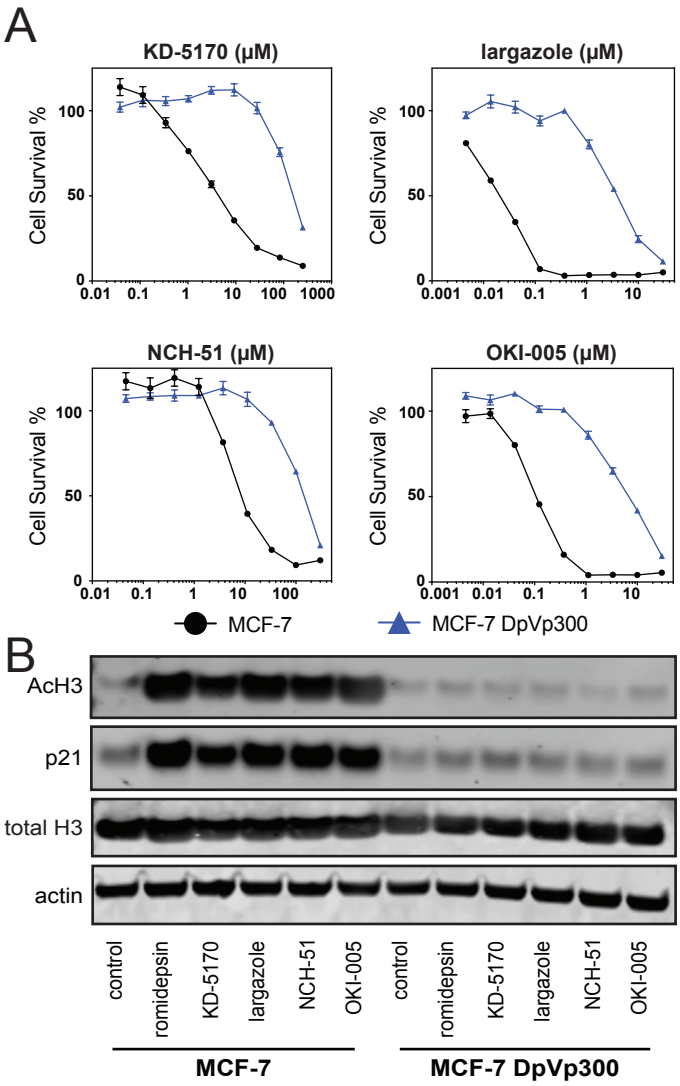
A
KD-5170 (μM)
largazole (μM)
NCH-51 (μM)
OKI-005 (μM)
Cell Survival %
MCF-7
MCF-7 DpVp300
B
AcH3
p21
total H3
actin
control
romidepsin
KD-5170
largazole
NCH-51
OKI-005
MCF-7
MCF-7 DpVp300

Figure 4

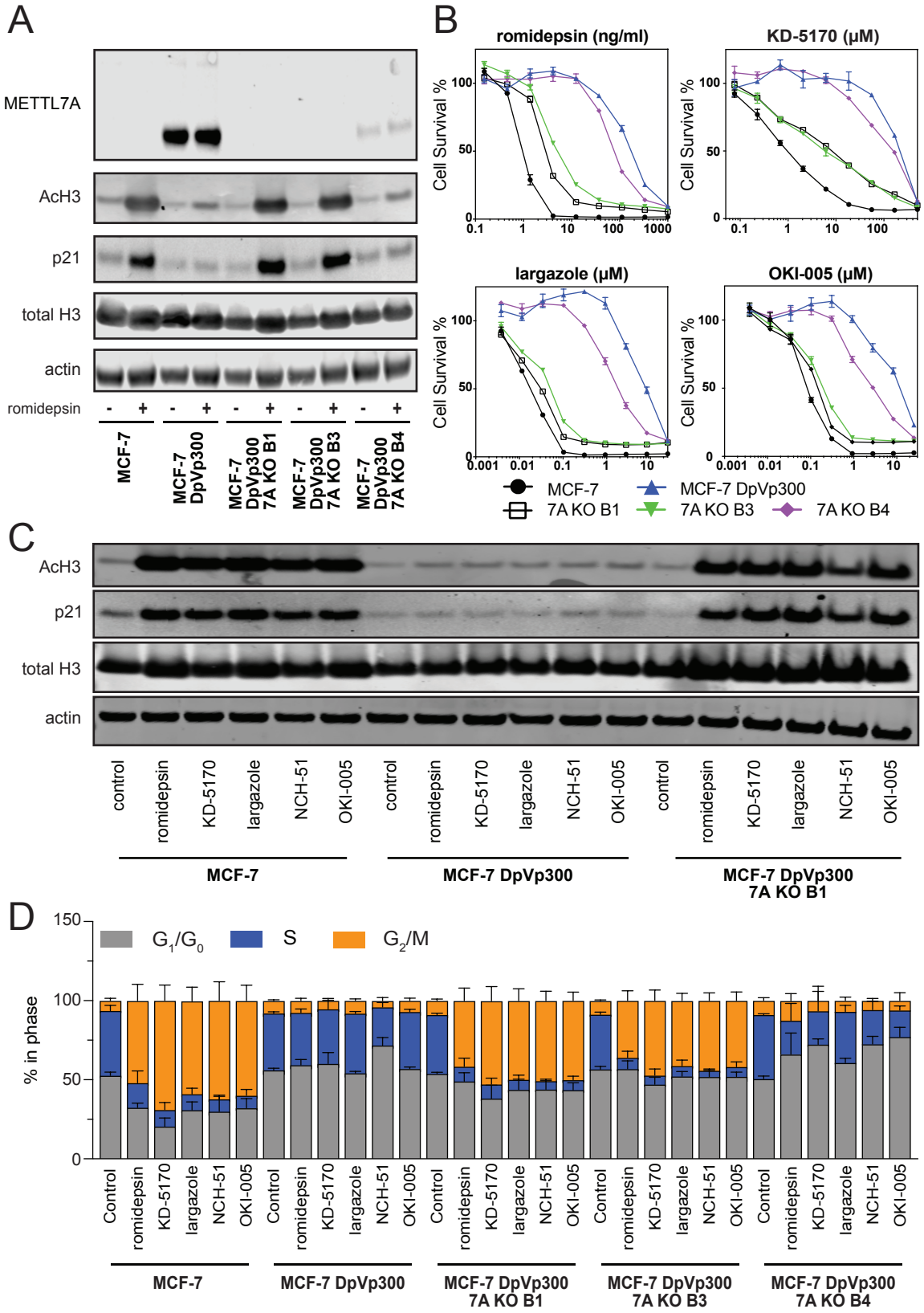
A
METTL7A
AcH3
p21
total H3
actin
romidepsin
MCF-7
MCF-7 DpVp300
MCF-7 DpVp300 7A KO B1
MCF-7 DpVp300 7A KO B3
MCF-7 DpVp300 7A KO B4
B
romidepsin (ng/ml)
KD-5170 (μM)
largazole (μM)
OKI-005 (μM)
Cell Survival %
MCF-7
MCF-7 DpVp300
7A KO B1
7A KO B3
7A KO B4
C
control
romidepsin
KD-5170
largazole
NCH-51
OKI-005
MCF-7
MCF-7 DpVp300
MCF-7 DpVp300 7A KO B1
D
% in phase
G1/G0
S
G2/M
Control
MCF-7 DpVp300 7A KO B3
MCF-7 DpVp300 7A KO B4

Figure 5

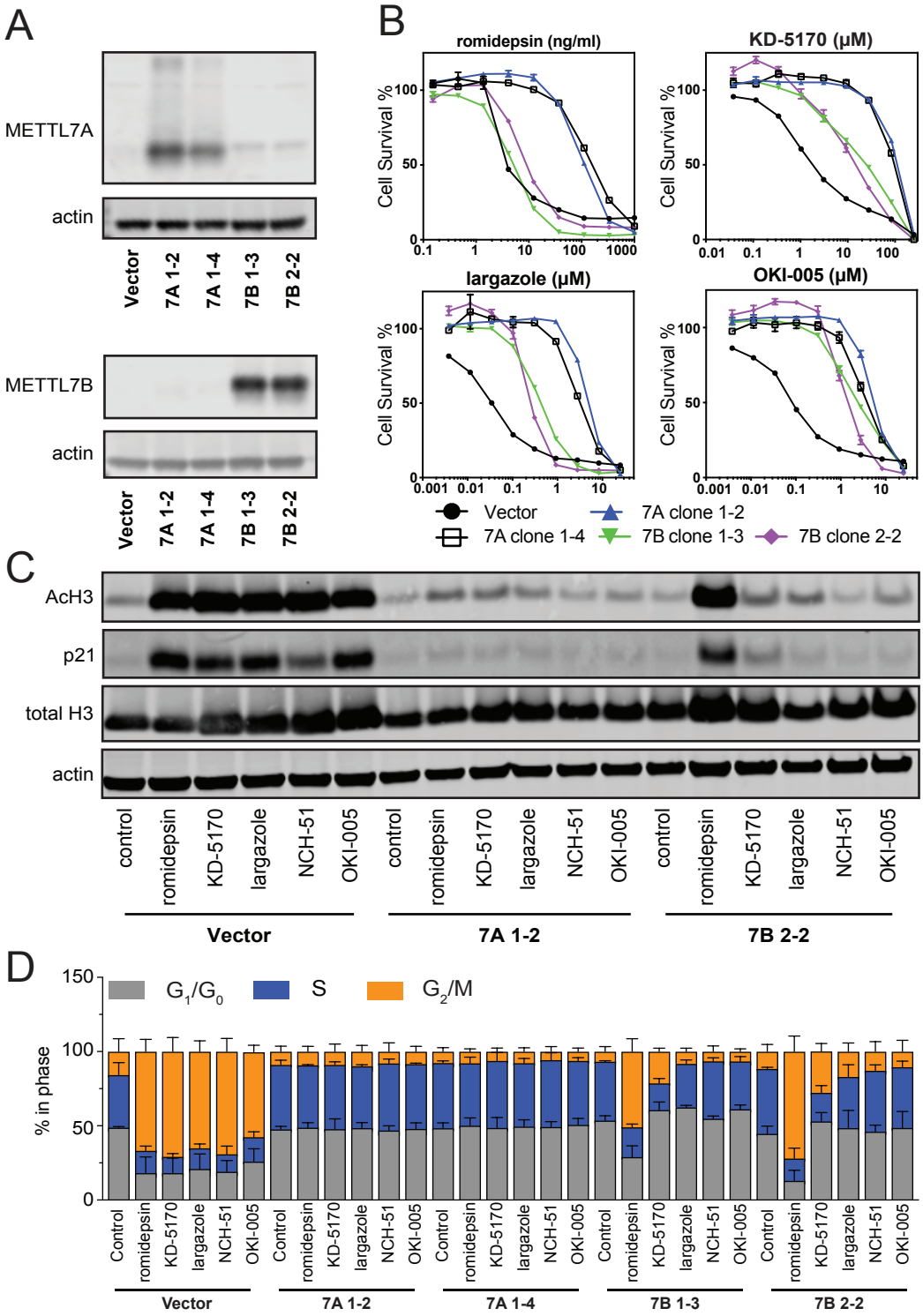
A
METTL7A
actin
Vector
7A 1-2
7A 1-4
7B 1-3
7B 2-2
METTL7B
actin
Vector
7A 1-2
7A 1-4
7B 1-3
7B 2-2
B
romidepsin (ng/ml)
KD-5170 (μM)
largazole (μM)
OKI-005 (μM)
Cell Survival %
Vector
7A clone 1-2
7A clone 1-4
7B clone 1-3
7B clone 2-2
C
AcH3
p21
total H3
actin
control
romidepsin
KD-5170
largazole
NCH-51
OKI-005
Vector
7A 1-2
7B 2-2
D
G1/G0
S
G2/M
% in phase
Control
romidepsin
KD-5170
largazole
NCH-51
OKI-005
Vector
7A 1-2
7A 1-4
7B 1-3
7B 2-2

Figure 6

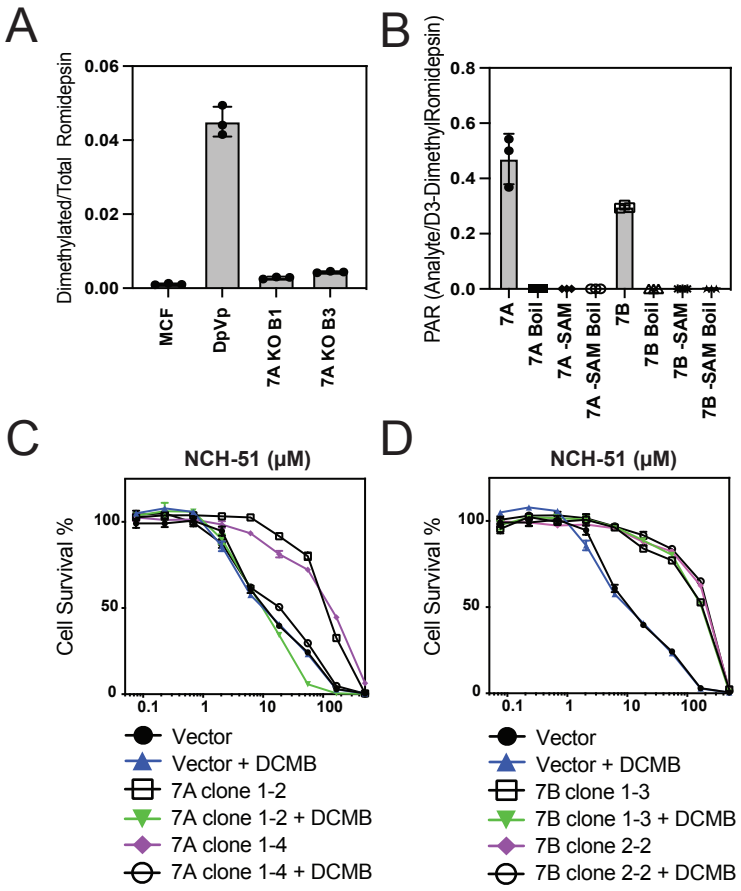
A
Dimethylated/Total Romidepsin
0.06
0.04
0.02
0.00
MCF
DpVp
7A KO B1
7A KO B3
B
PAR (Analyte/D3-DimethylRomidepsin)
0.8
0.6
0.4
0.2
0.0
7A
7A Boil
7A -SAM
7A -SAM Boil
7B
7B Boil
7B -SAM
7B -SAM Boil
C
NCH-51 (μM)
Cell Survival %
100
50
0
0.1
1
10
100
Vector
Vector + DCMB
7A clone 1-2
7A clone 1-2 + DCMB
7A clone 1-4
7A clone 1-4 + DCMB
D
NCH-51 (μM)
Cell Survival %
100
50
0
0.1
1
10
100
Vector
Vector + DCMB
7B clone 1-3
7B clone 1-3 + DCMB
7B clone 2-2
7B clone 2-2 + DCMB

Figure 7

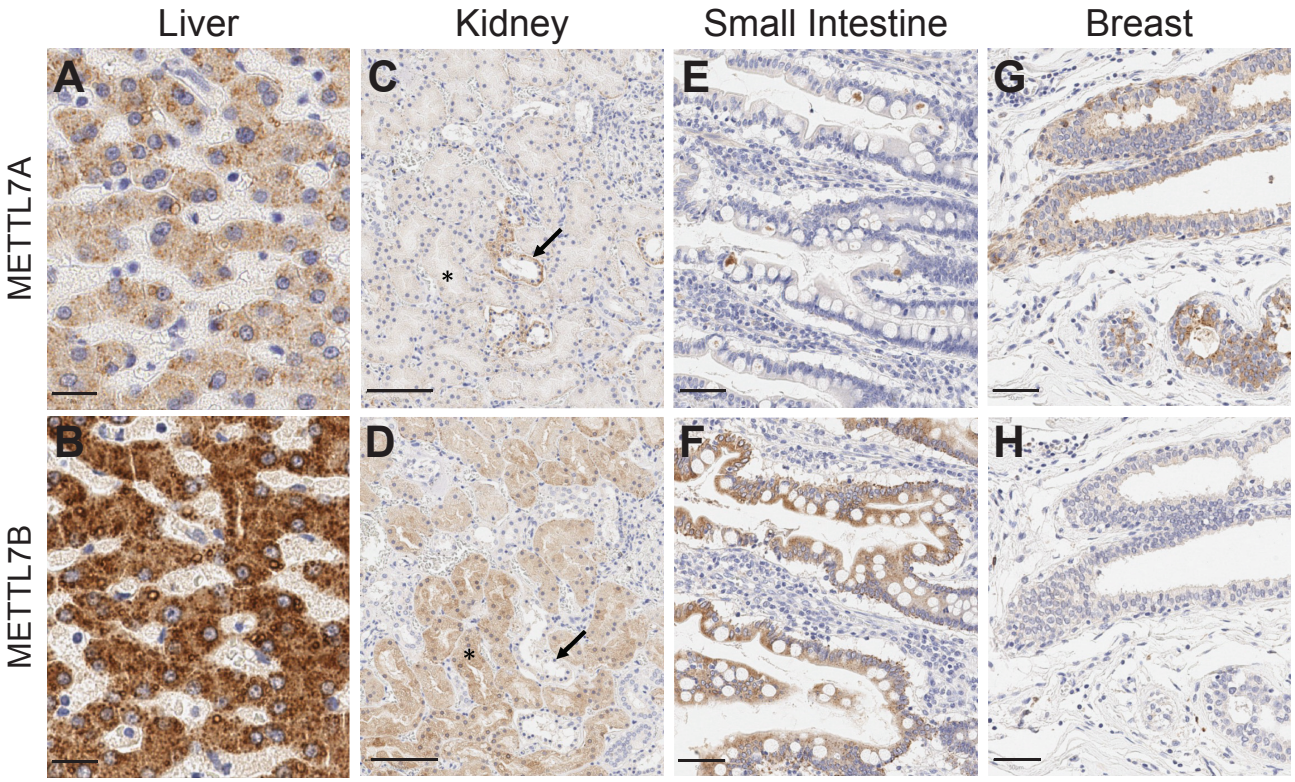
Liver
Kidney
Small Intestine
Breast
METTL7A
METTL7B
A
B
C
D
E
F
G
H

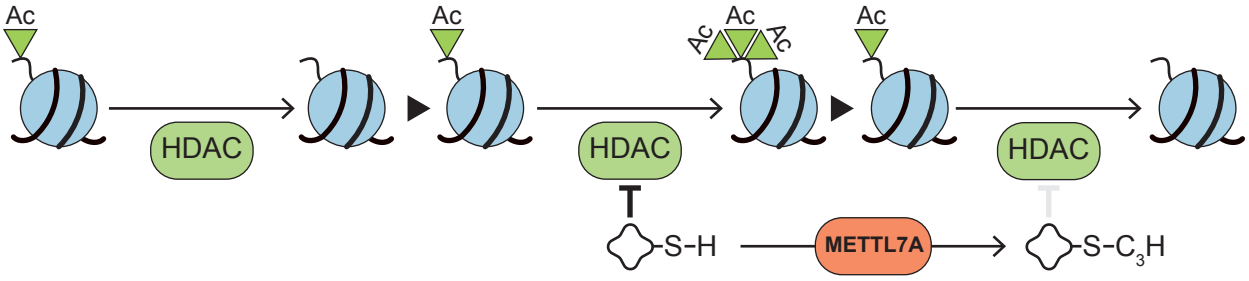
I
Ac
HDAC
Ac
HDAC
Ac
Ac
Ac
Ac
HDAC
S-H
METTL7A
S-C3H

Supplemental Figure 1

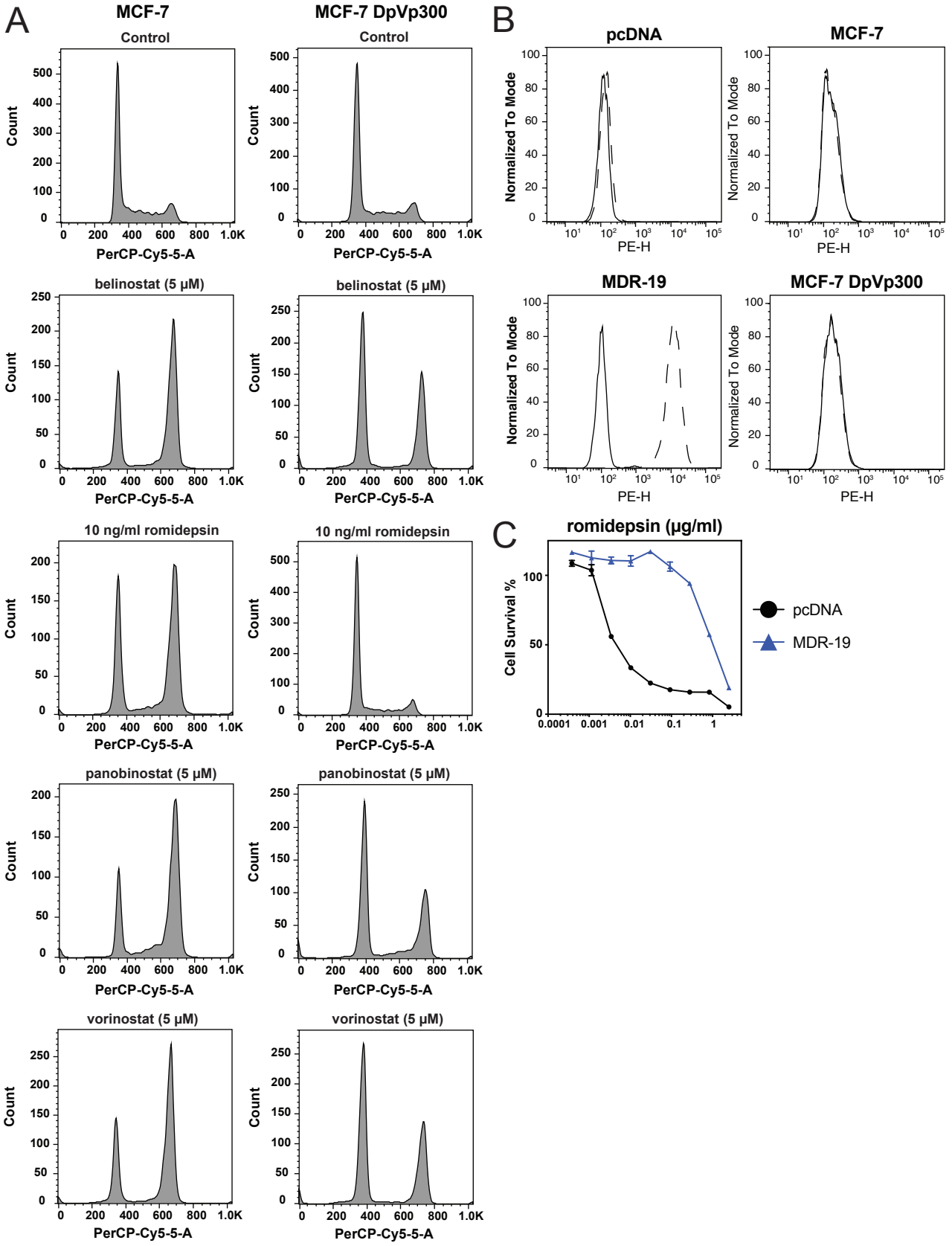

Supplemental Figure 2

A

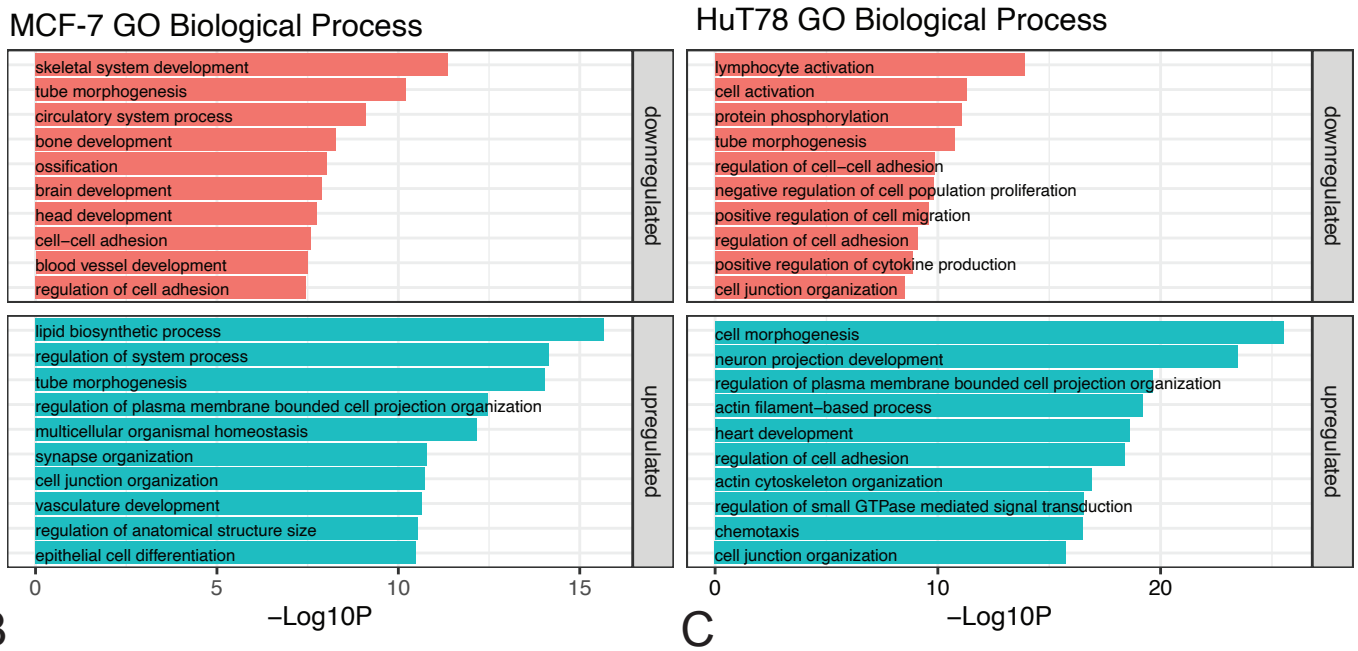

B

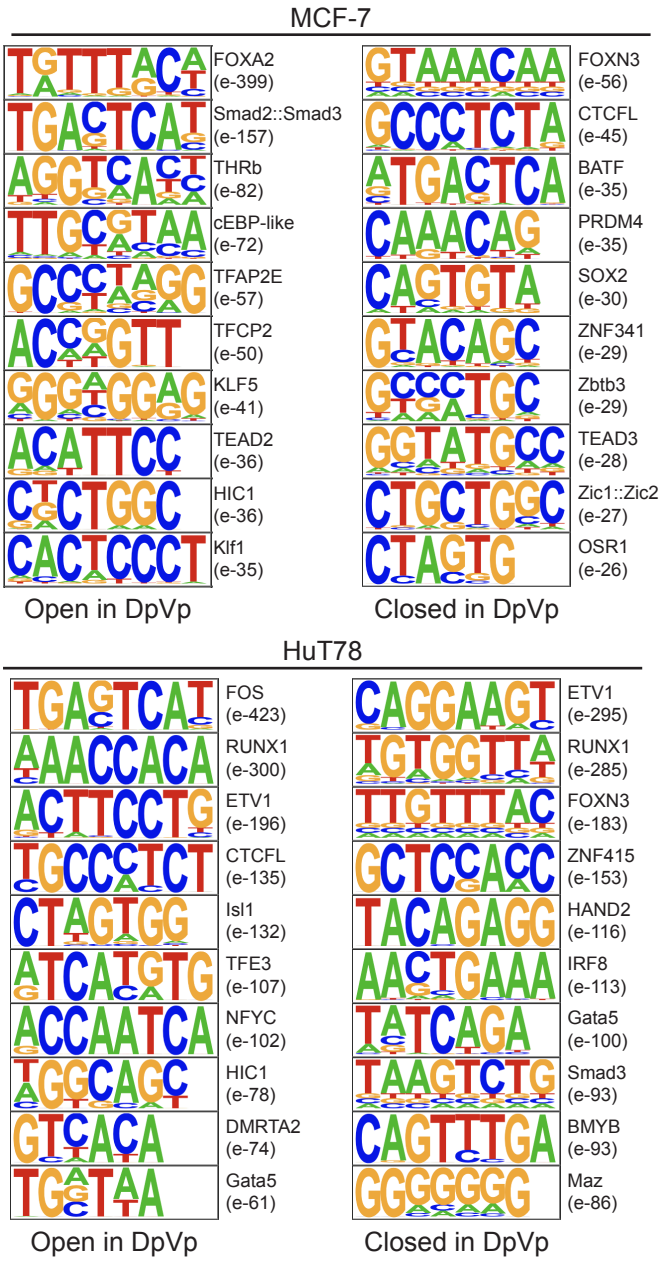

C

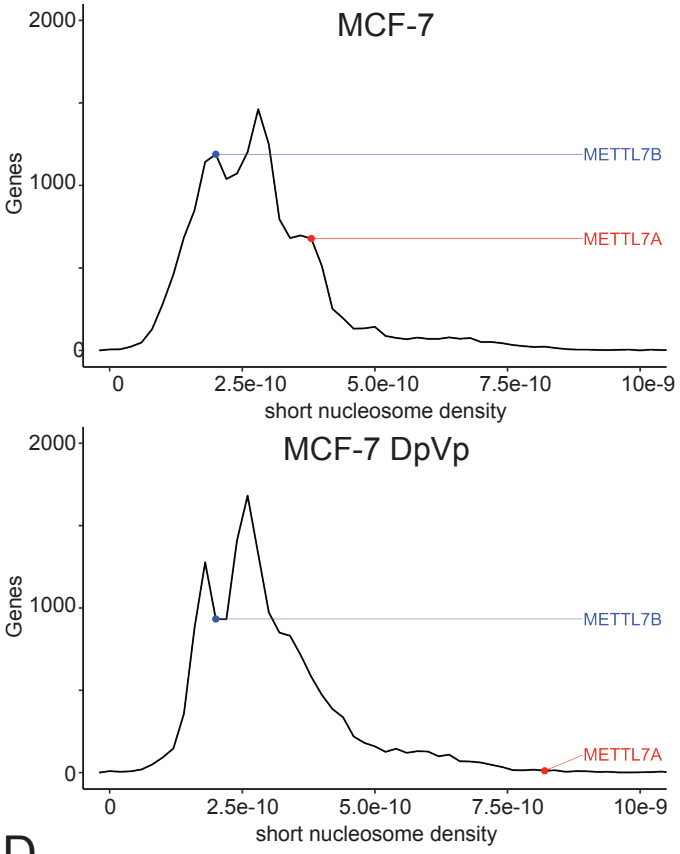

D

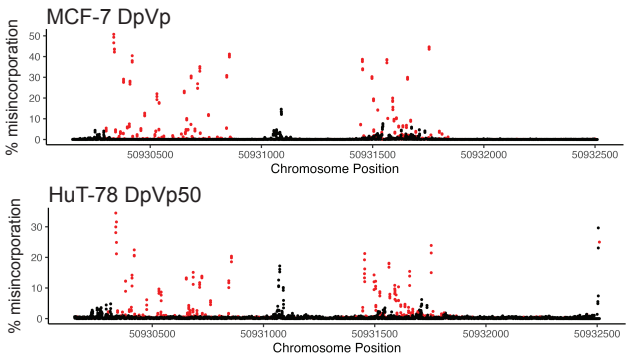

Supplemental Figure 3

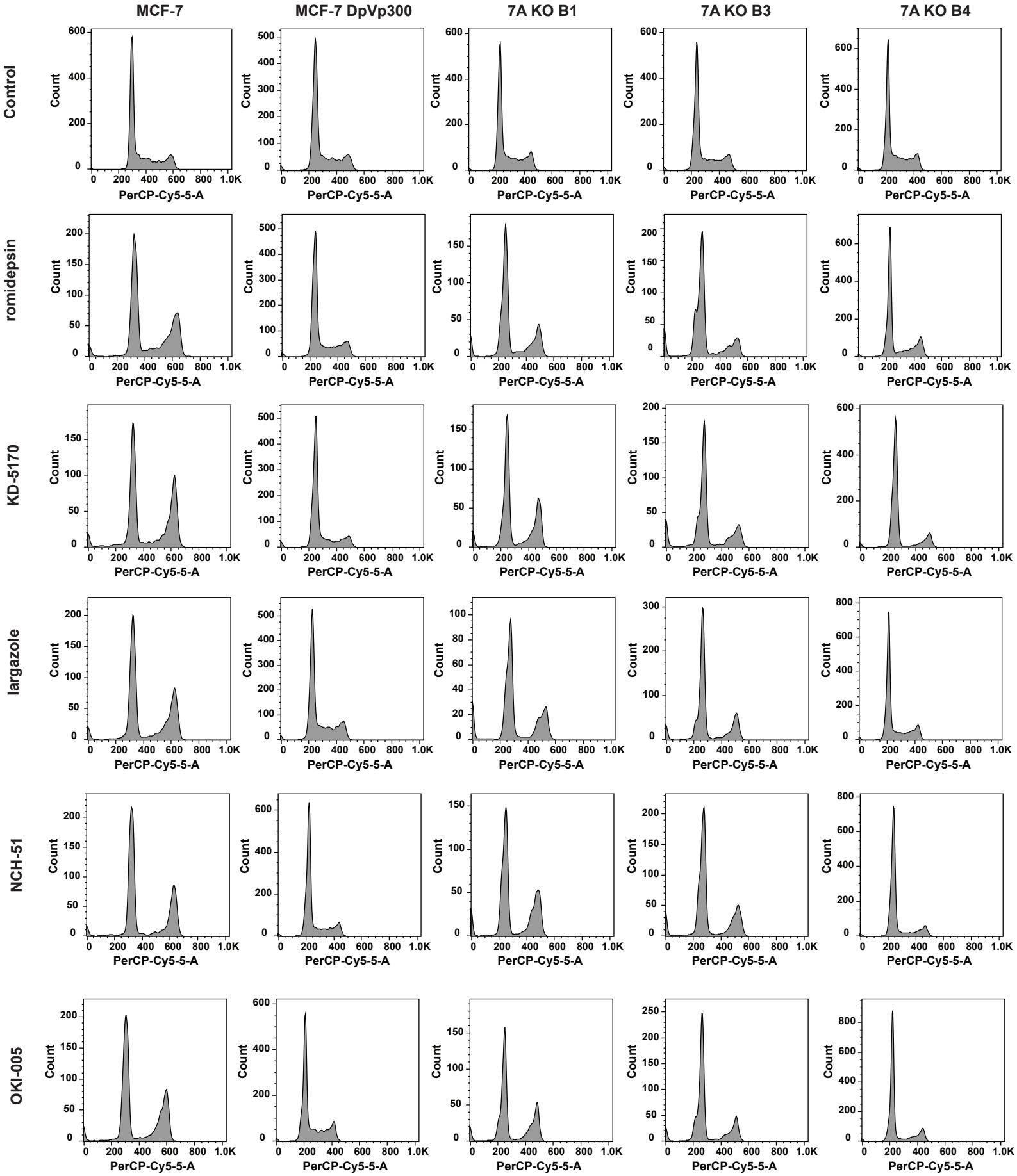

Supplemental Figure 4

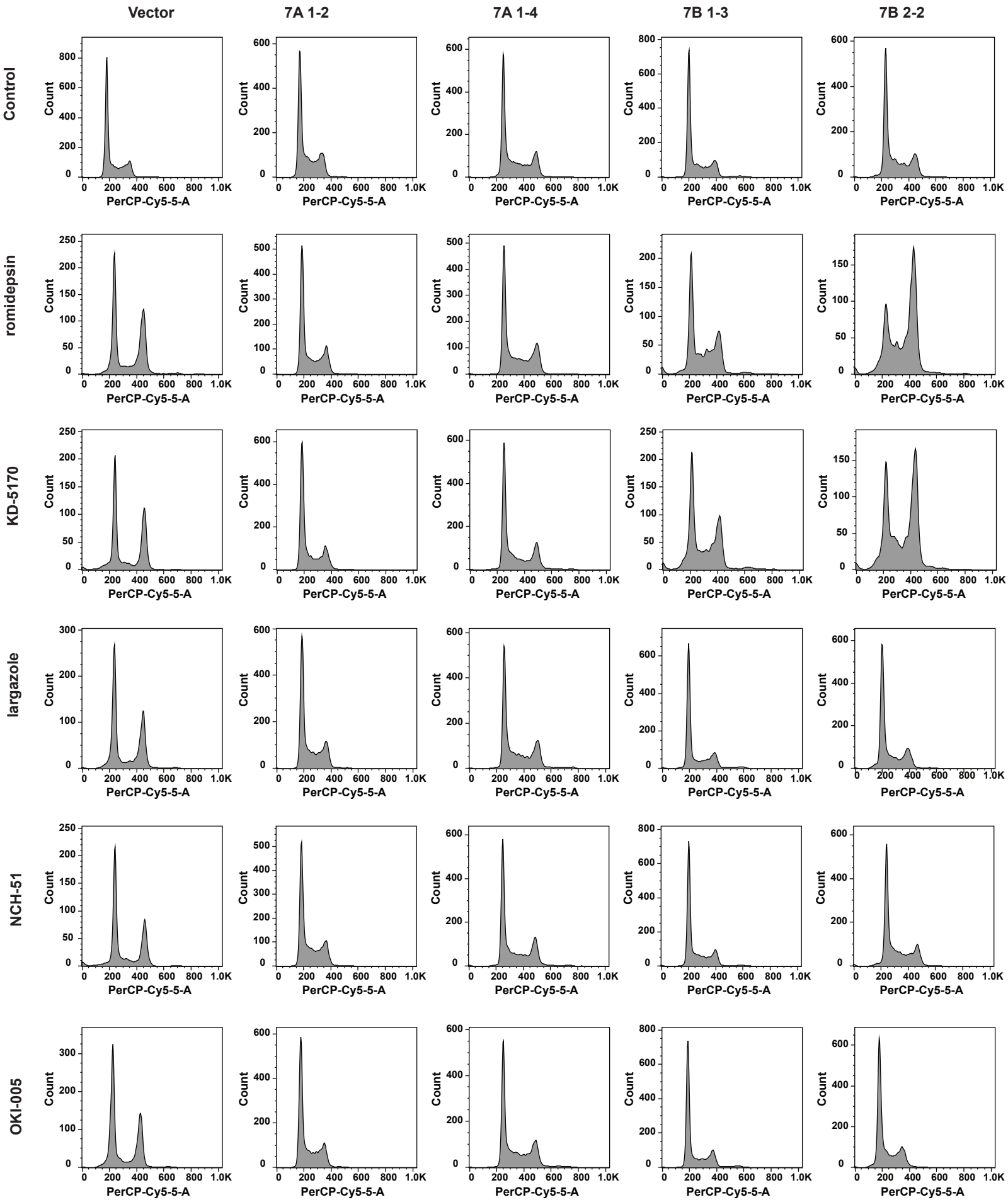

1073 **Supplemental Table S1. Cross resistance profile of MCF-7 DpVp300 cells**
1074

Drug	n	MCF-7	MCF-7 DpVp300	RR
Romidepsin (ng/ml)	10	1.7±0.10	361±33	212
Belinostat (μM)	3	0.57±0.067	4.7±0.93	8.4
Panobinostat (μM)	3	0.025±0.0065	0.063±0.0012	2.5
Vorinostat (μM)	3	1.4±0.056	6.8±0.84	4.8
Entinostat (μM)	3	2.1±0.25	18±9.3	8.1
Chidamide (μM)	4	15±0.69	49±1.9	3.3
Pracinostat (μM)	3	0.53±0.033	2.6±0.68	4.9
Mocetinostat (μM)	5	1.1±0.037	13±3.1	12
Dacinostat (μM)	3	0.063±0.0033	0.45±0.14	7.5
Rocilinostat (μM)	4	5.6±0.16	25±1.9	4.5
Apicidin (μM)	3	0.59±0.26	2.8±1.3	4.7
Resminostat (μM)	5	2.3±0.33	7.6±1.1	3.3
Trichostatin A (μM)	5	0.051±0.0055	0.16±0.014	3.1
PCI 34051 (μM)	5	12±1.8	23±1.1	1.9
Methotrexate (μM)	4	0.023±0.0035	0.028±0.0035	1.4
Topotecan (μM)	4	2.0±0.14	2.9±0.16	1.4
Teniposide (μM)	3	6.3±0.90	18±3.5	2.9
5-fluorouracil (μM)	3	122±6.0	199±17	1.6

1075
1076
1077 Results presented are mean GI_{50} values +/- SEM. Relative resistance (RR) value was
1078 determined by dividing the GI_{50} value for the MCF-7 DpVp300 cells by the GI_{50} value for
1079 the MCF-7 cells.
1080

1081

1082 **Supplemental Table S2. Cross resistance profile of MCF-7 DpVp300 cells with**
1083 **thiol-based HDACIs**
1084

Drug	n	MCF-7	DpVp300	RR
KD5170	3	4.9±1.3	173±11	35
Largazole	3	0.020±0.0015	7.1±4.3	355
NCH-51	3	9.4±0.15	149±28	16
OKI-005	3	0.11±0.015	7.5±0.10	68

1085
1086
1087 Results presented are mean GI_{50} values +/- SEM. Relative resistance (RR) value was
1088 determined by dividing the GI_{50} value for the MCF-7 DpVp300 cells by the GI_{50} value for
1089 the MCF-7 cells.
1090

1091

1092 **Supplemental Table S3. The cross resistance profile of MCF-7, MCF-7 DpVp300,**
1093 **7A KO B1, 7A KO B3 and 7A KO B4 cells**
1094
1095

Drug	n	MCF-7	MCF-7 DpVp300	7A KO B1	7A KO B3	7A KO B4
Romidepsin (ng/ml)	4	1.0±0.085	240±31	3.3±0.24	5.1±0.27	74±4.1
KD-5170 (μM)	3	1.1±0.21	234±24	9.7±1.8	8.9±2.2	193±43
Largazole (μM)	3	0.014±0.0027	9.6±0.48	0.026±0.0058	0.040±0.0075	2.1±0.18
NCH-51 (μM)	3	9.5±1.4	137±27	39±9.7	35±9.5	70±17
OKI-005 (μM)	3	0.085±0.0029	15±1.2	0.17±0.030	0.19±0.010	4.0±0.55
Vorinostat (μM)	4	2.7±0.62	7.6±1.2	5.6±0.39	5.7±0.67	5.3±0.49

1096
1097 Results presented are mean GI_{50} values +/- SEM.

1098

1099 **Supplemental Table S4. The cross resistance profile of Vector, 7A 1-2, 7A 1-4, 7B**
1100 **1-3 and 7B 2-2 cells**
1101
1102

Drug	n	Vector	7A 1-2	7A 1-4	7B 1-3	7B 2-2
Romidepsin	3	3.5±0.50	104±21	149±17	4.5±0.74	8.0±1.5
KD-5170	5	4.2±1.0	134±12	133±9.7	40±7.1	47±13
Largazole	3	0.049±0.011	4.9±0.34	5.6±1.5	0.51±0.042	0.42±0.073
NCH-51	3	7.5±1.7	103±12	71±17	182±47	117±31
OKI-005	3	0.14±0.032	5.6±0.30	6.5±1.4	2.8±0.40	2.3±0.40
Mocetinostat	4	0.89±0.084	0.72±0.11	0.90±0.077	1.0±0.17	0.78±0.066
Vorinostat	3	1.1±0.19	0.90±0.076	1.4±0.12	1.2±0.088	1.2±0.058

1103
1104 Results presented are mean GI_{50} values +/- SEM.

1105

1106 **Supplemental Table S5. Normal tissue expression of METTL7A and METTL7B**
1107

Tissue	METTL7A positive samples	METTL7B positive samples
Brain	9/14	9/14
Testis	15/15	15/15
Prostate	0/5	0/5
Ovary	0/7	0/7
Breast	5/5	0/5
Cervix	0/5	0/5
Heart	10/10	10/10
Kidney	15/15	15/15
Liver	13/14	13/14
Lung	0/15	0/15
Pancreas	0/5	0/5
Esophagus	0/5	0/5
Stomach	15/15	15/15
Small intestine	0/4	4/4
Colon	0/13	10/13
Rectum	0/5	1/5
Skin	3/3	3/6
Lymph node	0/5	0/5
Spleen	0/16	0/16
Bone marrow	0/5	0/5
Thymus	0/5	0/5

1108
1109

1110 **Supplemental Table S6: Staining methods and antibodies for**
1111 **immunohistochemistry**
1112

Antibody	Dilution	Antigen Retrieval	Secondary Antibody kit	Control Tissue	Manufacturer	Catalog Number
METTL7A	1:500	Citrate 20’	Bond polymer refine kit (minus postprimary reagent)	Empty vector and *METTL7A* transfected HEK-293 cells	Origene	TA346478 (rabbit polyclonal)
METTL7B	1:500	Citrate 20’	Bond polymer refine kit (minus postprimary reagent)	Empty vector and *METTL7B* transfected HEK293 cells	Sigma	HPA830644 (rabbit polyclonal)

1113